SENTINEL 2

S2 MPC

Level-2A Algorithm Theoretical Basis Document

Ref. S2-PDGS-MPC-ATBD-L2A

Authors Table

	Name	Company	Responsibility	Date	Signature
Written by	J. Louis & L2A team	TPZ F	ESL L2A Leader	2021-11-15	
Verified by	O Devignot	CS	Quality Manager	2021-11-15	
Approved by	L. Pessiot	CS	Service Manager	2021-11-15	

Change Log

Issue	Date	Reason for change	Pages(s)/Section(s)
2.3	2016-12-23	Creation – S2MPC template update and alignment with Sen2Cor v2.3.0 processing	all
2.4	2017-12-14	Updated atmospheric correction part, included using ECMWF AOT information for non-DDV granules	Section 4
2.5	2018-05-31	Updated scene classification part in line with Sen2Cor 2.5.5	Section 3
2.9	2021-04-09	Updated atmospheric correction part, Updated scene classification part in line with Sen2Cor 2.9.0	Section 3 Section 4
2.10	2021-11-15	Updated scene classification part in line with Sen2Cor 2.10.0	Section 3

Table of contents

1. Introduction

1.1 Purpose of the document

This Algorithm Theoretical Basis Document (ATBD) describes the algorithms implemented in atmospheric correction processor Sen2Cor. In the current approach Sen2Cor is designed for working on mono-temporal Copernicus Sentinel-2 imagery over land. Copernicus Sentinel-2A and -2B MSI are the high spatial Resolution (HR) optical payloads of the Copernicus program.

Level 2A processing with Sen2Cor is mainly performed by two parts:

- Scene classification (SC): the generation of a scene classification map and of two quality indicators: (1) A map of cloud probability and (2) a map of snow probability. They are additional products and serve as a necessary input for the atmospheric correction part. SC is described in chapter 3 of this document.

- Atmospheric correction (AC): this algorithm has to be performed in order to obtain Bottom of Atmosphere (BOA) corrected transforms of multispectral Level 1C (L1C) products. L1C products cover Top of Atmosphere (TOA) reflectance images. For this transformation, a database of look-up tables (LUTs) was compiled using the atmospheric radiative transfer model libRadtran1 [1, 2]. The LUTs were generated according to the Sentinel-2 spectral responses, in order to obtain the sensor-specific functions needed for the atmospheric correction, i.e. path radiance, direct and diffuse transmittances, direct and diffuse solar fluxes, and spherical albedo. The AC part is described in chapter 4 of this document.

Sen2Cor is used in operational environment of Sentinel-2-PDGS for global processing and generation of ESA-L2A core product, which can be downloaded from OpenHub [https://scihub.copernicus.eu/dhus/]. Sen2Cor can also be downloaded from http://step.esa.int/main/third-party-plugins-2/sen2cor/ for L2A-generation by the user. Differences between both processing chains and recommendations for processing configurations are given in Sen2Cor Configuration and User Manual [S2-L2A-SUM]. A complete list of configuration parameters contains [S2-L2A-IODD].

Restrictions:

1. The current processing baseline and processor version are not designed for applications over water or on coastal regions. The processor doesn't contain modules for correction of water surface effects like sunglint. Both Aerosol optical thickness (AOT) and Water vapour (WV) are not estimated over water surface. However, the current implementation does not prevent an application over water using AOT and WV from the nearby land surface and doing without correction of surface effects.

[1] libRadtran - library for radiative transfer - is a collection of C and Fortran functions and programs for calculation of solar and thermal radiation in the Earth's atmosphere. libRadtran is freely available under the GNU General Public License. The libRadtran release used to compute the LUTs is: 2.0.2

1.2 Document Structure

The document is structured as follows:

The remaining part of this chapter reviews and summarizes the relevant Copernicus Sentinel-2 documentation to assess the prerequisites of the L2A processing.

Chapter 0 lists the sensor characteristics which are the common base for the next two chapters 3 and 4. It gives also an introduction to the processing chain.

Chapter 3 describes the algorithms proposed to detect clouds, snow and cloud shadows, and to generate a scene classification mask and associated quality indicators.

Chapter 4 contains a detailed theoretical description of each retrieval algorithm for the atmospheric correction (cirrus removal, aerosol, water vapour, and surface reflectance retrieval in flat and rugged terrain). The chapter finishes with a proposed processing strategy for the AC part.

The appendix lists a collection of relevant documentation, which forms the scientific background of the algorithms described before.

1.3 References

Document ID	Description	Version
S2-PDGS-MPC-L2A-PFS	Sentinel-2 MSI – Product Format Specification	14.6
S2-PDGS-MPC-L2A-SUM	Sentinel-2 MSI – Level 2A Prototype Processor Installation and User Manual	2.9
S2-PDGS-MPC-L2A-IODD	Sentinel-2 MSI – Level 2A Prototype Processor Input Output Definition Document	2.9
S2-PDGS-MPC-L2A-DPM	Sentinel-2 MSI – Level 2A Detailed Processing Model	1.0
S2-PDD	GMES Space Component – Sentinel-2 Payload Data Ground Segment (PDGS), Product Definition Document	2.3
S2-PSD	Sentinel-2 Products Specification Document	14.6
CAMS	FTP access to CAMS global data: link: FTP+access+to+CAMS+global+data	N/A

2. Sensor Characteristics, I/O data

Copernicus Sentinel-2A and Sentinel-2B were launched into a sun-synchronous orbit at 786 km. The MSI instrument covers a 290 km swath allowing a revisit time of 10 days and resulting in 5 days revisit time with the two satellites. Data encoding is 15 bits/pixel and the radiometric accuracy is within 5% requirement, for most bands within 3% goal [3].

2.1 Sensor specification

The sensor has three different spatial resolutions (10 m to 60 m) and 13 spectral bands as shown in Figure 2-1.

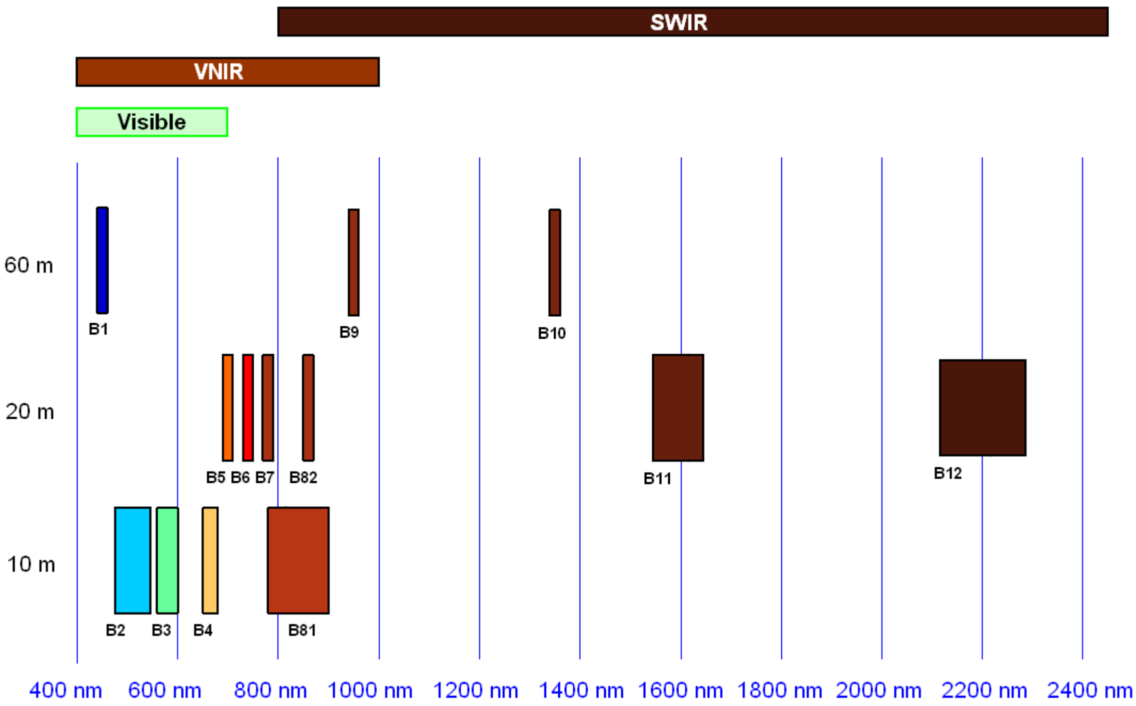

Figure 2-1 – S2/MSI spectral bands and resolutions

The three 10 m bands in the visible region enable true colour images with a high spatial resolution, which is especially important for urban areas. The 10 m wide NIR band also allows a 10 m false colour infrared (CIR) composite. Spectral bands needed to retrieve atmospheric parameters are designed with a coarser resolution of 60 m (bands at 443 nm, 940 nm, 1375 nm) which is justified because aerosol, water vapour, and cirrus contents usually do not vary rapidly within a scale of 100 m. The remaining bands have a spatial resolution of 20 m. Figure 2-2 shows the normalized spectral filter functions of the Sentinel-2A and Sentinel-2B bands [4].

All VNIR bands are influenced by aerosol scattering. Ozone absorption mostly influence the signal in bands 2 - 5, bands 5, 8 and 12 slightly depend on the atmospheric water vapour column and band 9 measures the water vapour absorption depth [Figure 2-3]. CO_2 absorption in band 11 and Methane absorption in band 12 are weak enough to be accounted for in the LUTs with climatological absorber amount. Variations of absorber amounts for CO_2 and Methane over the globe are small compared to variations of ozone and WV columns.

The sensor characteristics are summarized in Table 2-I.

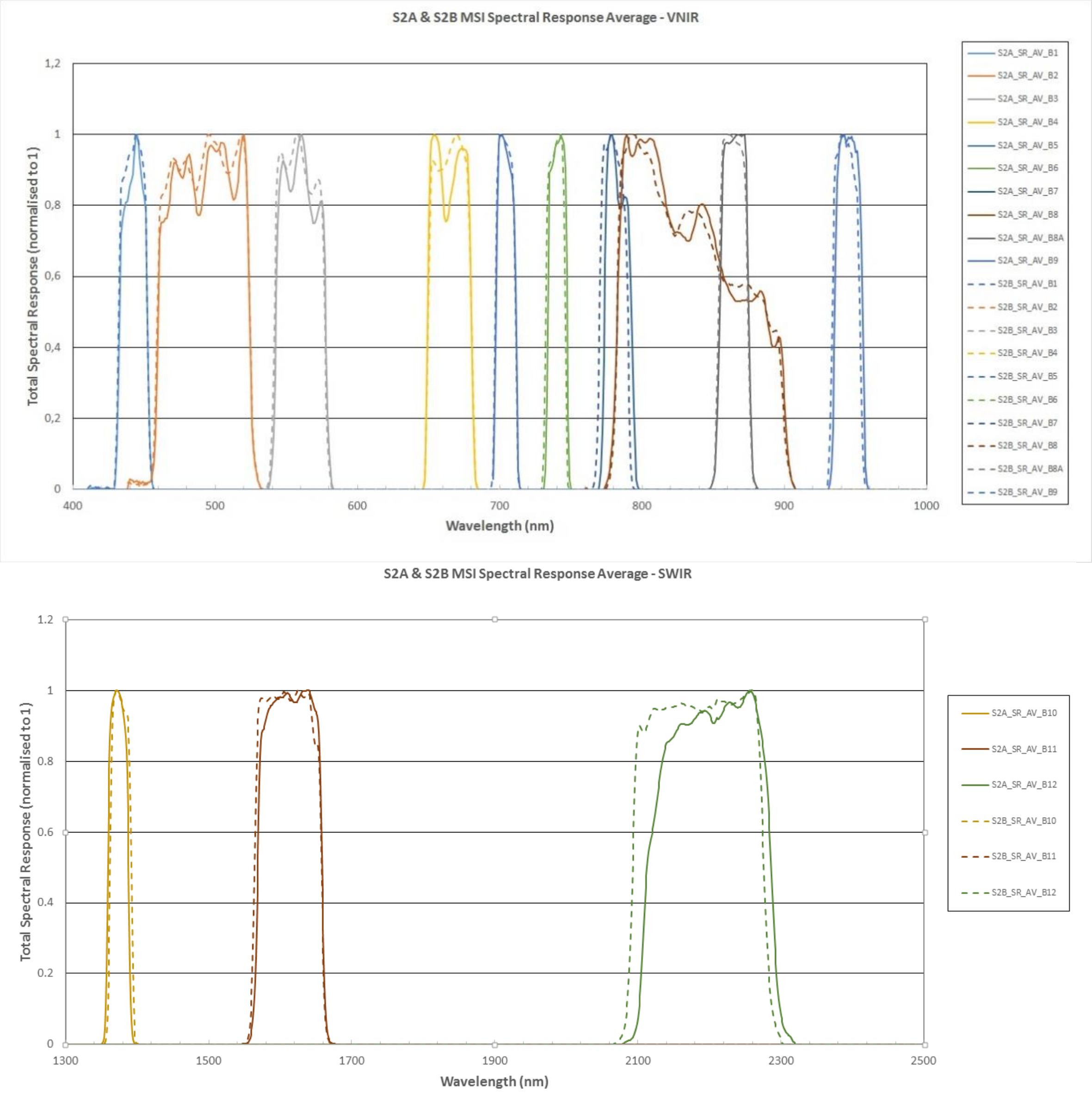

Figure 2-2 – S2A and S2B (dashed) filter curves

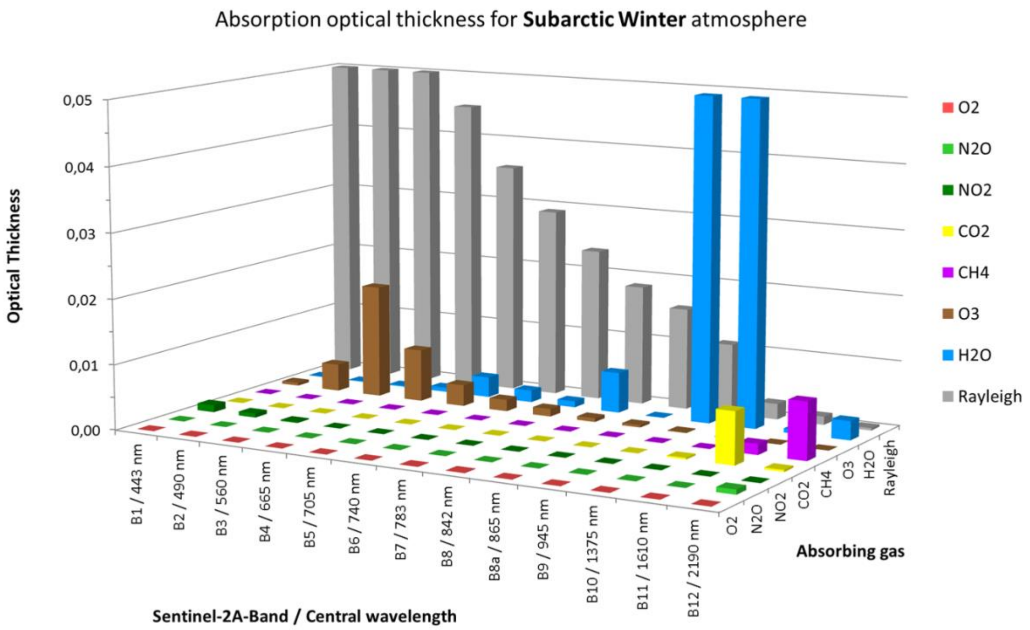

Figure 2-3 – Absorption optical thickness for S2A-bands for different absorbers and the subarctic winter atmosphere resulting from MODTRAN [5] absorption models

Table 2-I – Spectral bands of Sentinel-2, spatial resolution and purpose

Band	Center λ (nm)`	Spectral Width Δλ (nm)	Spatial Resolution (m)	Purpose in L2A processing context
B1	443	20	60	Atmospheric Correction (coastal blue)
B2	490	65	10	Sensitive to Vegetation Aerosol Scattering (blue)
B3	560	35	10	Green peak, sensitive to total chlorophyll in vegetation (green)
B4	665	30	10	Max Chlorophyll absorption (red)
B5	705	15	20	Vegetation Red Edge 1
B6	740	15	20	Vegetation Red Edge 2
B7	783	20	20	Vegetation Red Edge 3
B8	842	115	10	Leaf Area Index (LAI)
B8a	865	20	20	Used for water vapour absorption reference
B9	945	20	60	Water Vapour absorption atmospheric correction
B10	1375	30	60	Detection of thin cirrus for atmospheric correction
B11	1610	90	20	Soils detection
B12	2190	180	20	AOT determination

2.2 Input data

All input data of the processor are listed in section 2.1.1 (Input Data) of the according Product Definition Document [S2-L2A-PDD].

2.3 Output data

All output data of the processor are listed in section 2.1.2 (Product Summary) of the according Product Definition Document [S2-L2A-PDD].

2.4 L2A Processing Strategy

Sen2Cor is designed for processing on granule level in the current approach. It should be known that small surface reflectance brightness steps at granule borders might occur if several granules are connected to one larger image because of the independent processing of each granule. They have to be accepted as long as processing on granule base is technically unavoidable. Brightness steps can be minimized by configuration of Sen2Cor to avoid change of the aerosol type and profile between successive scenes. This is also recommended for processing of time series. Recommendations for configuration of Sen2Cor can be found in Sen2Cor Configuration and User Manual [S2-L2A-SUM].

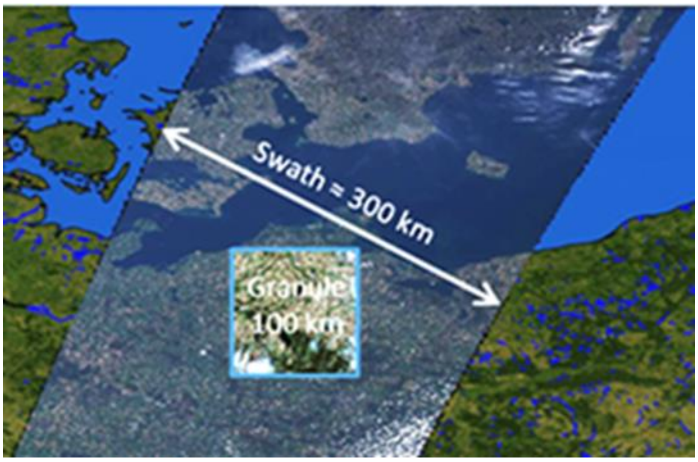

Figure 2-4 – Location of a tile in a Sentinel-2 data strip

All algorithms described in this document are performed on a per-pixel basis. As the bands used in the SC and AC algorithms have different resolutions (see Table 2-1) parts of the bands need to be resampled[2]. The precision of the algorithms is always dependent on the lowest resolution provided.

[2] For the down sampling (i.e. from 10 m to 20 m resolution) a method based on block means is used whereas for up sampling (i.e. from 60 m to 20 m resolution) a cubic spline method is used. SCL map is resized from 20m to 60m with an order of 0 for spline interpolation, in order to keep the classification values.

2.4.1 Sen2Cor processing chain

Figure 2-5 shows a general overview of the Sen2Cor processing chain. First, the scene classification is performed on basis of TOA orthorectified L1C-data. It is recommended to use CCI-data and a DEM as auxiliary inputs to scene classification. Information about installation and setup of the ESACCI-LC for Sen2Cor data package can be found in [S2-L2A-SUM] and supported DEM format can be found in [S2-L2A-IODD]. After scene classification a cirrus correction can follow, which is an optional pre-processing step performed also on TOA-data. Atmospheric correction processing includes AOT and WV retrieval and uses this information to convert TOA reflectance cube to BOA reflectance cube. BOA reflectance cube is equivalent to surface reflectance. Atmospheric correction modules can also use a DEM as auxiliary input. Additionally they rely on pre-computed look-up tables.

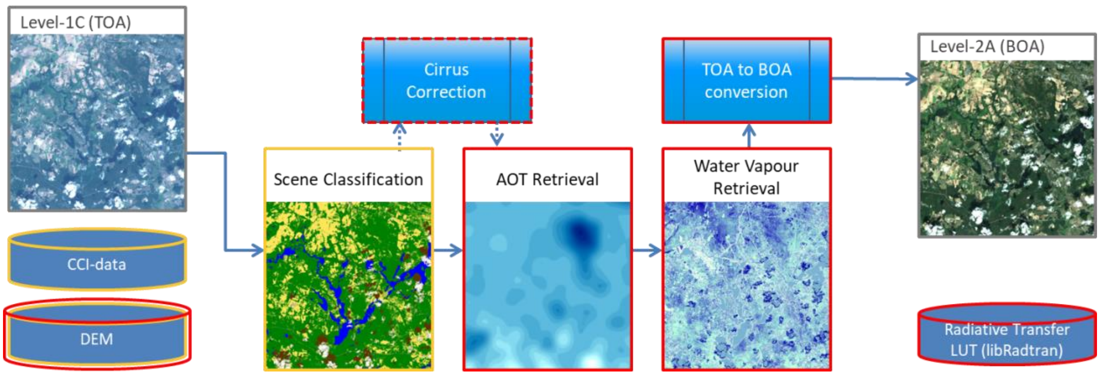

Figure 2-5 – Sen2Cor processing chain

Modules and auxiliary data belonging to scene classification are encircled by a yellow line. Red lines surround modules and data belonging to atmospheric correction part.

Missing, defective and saturated pixels are classified in advance of the scene classification algorithm and collected in two separate classes. They are excluded from further processing. Saturated pixels may disturb the calculation of the spectral band ratios and the actual meaning of the thresholds of the scene classification. Therefore they have to be identified and isolated from the algorithm before the computation of the spectral ratios. When L1C data is re-projected on granules (see Figure 2-6) it may occur that on the borders of the acquisition, data are missing on the granule. These non-existing data have also to be excluded from the processing.

Scene classification makes use of a series of threshold tests on L1C data, spectral band signals, band ratios and indices (as is specified in Chapter 3). The aerosol optical thickness (AOT) map is calculated using dark reference areas (see below), most preferably dense dark vegetation (DDV) pixels. Fall-back solutions are provided in case that the image doesn't contain sufficient reference pixels (as is specified in Chapter 4.3). Atmospheric Pre-corrected Differential Absorption Algorithm (APDA) [6] is implemented for Water Vapour (WV) retrieval. Vertical WV column is calculated with the band 8a (865 nm, 20 m spatial resolution) and band 9 (945 nm, 60 m resolution resampled to 20 m) (as is specified in Chapter 4.4). TOA to BOA conversion is specified in Chapters 4.5 to 4.8. A topographic correction is recommended for TOA to BOA conversion if more than 1% of the pixels have slopes > 6°. Otherwise, the terrain can be considered as flat using the average elevation which decreases the processing time by a factor of 3 to 4. Justification for the > 6° slope criterion: for a typical solar zenith angle of θs = 40° this approximately corresponds to a 8% variation of the direct local solar irradiance (i.e., $\cos(\theta_s - 6) / \cos(\theta_s) = 1.08$). TOA to BOA conversion also includes a correction of adjacency effect and an optional BRDF correction.

From an atmospheric correction point of view, the Sentinel-2 data processing could be performed to obtain a 60 m, a 20 m and a 10 m surface reflectance product. Figure 2-7 shows how default processing of the 60 m and 10 m products depend on 20 m processing. Whereas 60 m processing may also be independent, the 10 m processing needs the 20 m processing to be performed before.

Figure 2-6 – Level-1C data re-projection on tiles

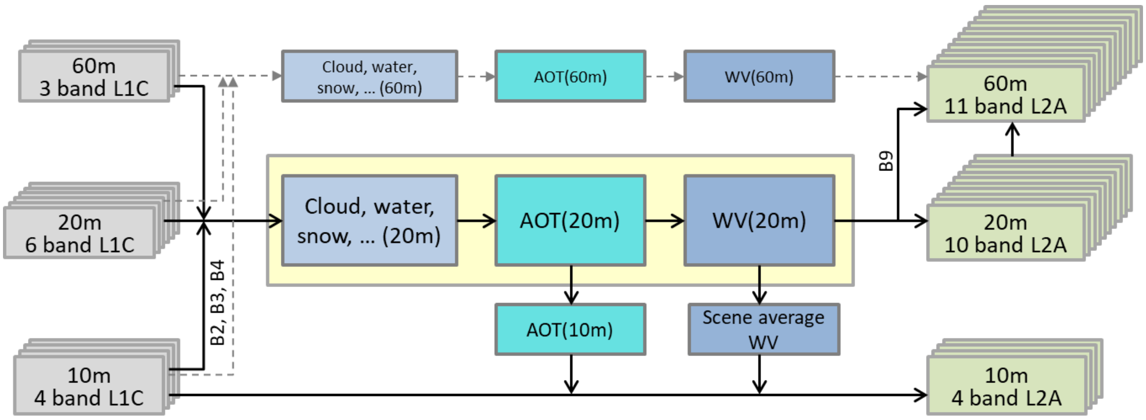

Figure 2-7 – Schematic sketch of processing the 60 m, 20 m, and 10 m data of Sentinel-2;
black solid arrows: default processing chain based on 20m data
grey dashed arrows: alternate 60m processing

2.4.2 L2A Processing at 60 m

All processing (SCL, AOT, WV) is done on 20m cube by default and can be resampled[2] to 60m output. Refer to 2.4.3 for processing at 20m spatial resolution. The output product at 60 m contains all of SCL, AOT and WV maps and a surface reflectance cube of 11 bands. Note, that 60 m output includes the WV band (B09), which is not provided in the 20 m output. The cirrus band (B10) is omitted as it does not represent surface information. The 60 m output product does not include the spectrally wide NIR band (B08) at 10 m resolution, because it doesn't contain additional information for 60m output compared to the spectrally narrower NIR band (B08A) given at 20 m spatial resolution. Default output also includes a True Colour Image (TCI) and snow- and cloud probability maps from the SCL in the QI_DATA folder. If explicitly specified by the user in Sen2Cor configuration file, then also the resampled DDV-map is provided within the QI_DATA folder of L2A-product and. If a DEM is used, output of the DEM resampled to 60 m spatial resolution into the AUX_DATA folder can be specified.

There is also an option for 60m processing (only) if the user specifies --resolution=60 in the command line. A complete SCL, AOT, WV, cirrus, and surface reflectance retrieval processing can then be performed for the 60 m data. Inputs to the atmospheric correction of the 60 m product are then: the coarse pre-classification (as is specified in Chapter 3) and a data file with 12 L1C-bands on tile level (all bands except the spectrally wide 10 m resolution NIR band, B08). The 10 m and 20 m bands are resampled to 60 m. In mountainous terrain, it is recommended to use a DEM. The DEM provided by the user (e.g. SRTM) is resampled internally to 60 m resolution because 60 m DEM is needed for the processing.

2.4.3 L2A Processing at 20 m

SCL processing is performed in 20 m spatial resolution. The 10 m and 60 m bands are resampled to 20 m. Inputs to the 20m atmospheric correction processing are the 20 m pre-classification map (land, water, cloud and snow/ice) and a data file with 12 L1C-bands on tile level (all bands except the spectrally wide 10 m resolution NIR band, B08). WV is calculated using band B8A data (865nm, with the original 20 m resolution) and band 9 (945 nm) data resampled to 20 m. In mountainous terrain, it is recommended to use a DEM. The DEM provided by the user (e.g. SRTM) is resampled internally to 20 m resolution.

The output product contains all of SCL, AOT and WV maps and a surface reflectance cube of 10 bands at 20 m spatial resolution – all native 20 m spatial resolution bands and the B01 up sampled. The cirrus band (B10) and WV band (B09) are omitted as they do not provide surface information usable for downstream applications. B08 is not contained in the 20 m output for the same reason as for the 60 m output. B08A in its native 20 m spatial resolution represents the surface reflectance better because it is spectrally narrower. Default output also includes a TCI image and snow- and cloud probability maps from the SCL in the QI_DATA folder. If explicitly specified by the user in Sen2Cor configuration file, then also the DDV-map is provided within QI_DATA folder of L2A-product. If a DEM is used, output of the DEM resampled to 20 m spatial resolution into the AUX_DATA folder can be specified.

2.4.4 L2A Processing at 10 m

This processing involves four bands (B02, B03, B04, B08, i.e., blue, green, red, spectrally broad NIR-band). Inputs are the previously calculated SCL (20 m), AOT (20 m) and WV (20 m) which have to be resampled to get SCL (10 m), AOT (10 m) and WV (10 m). Also the DEM provided by the user for processing in rugged terrain is internally resampled to 10 m. No AOT and WV retrieval are performed at 10 m spatial resolution. Scene-average water vapour is used during the surface reflectance retrieval as only B08 is affected a little by WV absorption and the water vapour influence is very small. WV column in the LUT nearest to scene-average WV specifies the LUT file name used for processing. Example: the scene-average value is 1.4 cm, and LUTs are provided for water vapour columns of 0.4, 1.0, 2.0, 2.9, 4.0, and 5.0 cm. Then the LUT file name corresponding to 1.0 cm is specified in the input parameter file.

The output product contains up scaled AOT and WV maps, a surface reflectance cube of all 4 native 10 m spatial resolution bands and a TCI-image. If a DEM is used, output of the DEM resampled to 10 m spatial resolution into the AUX_DATA folder can be specified.

3. Scene Classification

3.1 Overview

The scope of the algorithm described in this chapter is to detect clouds, snow and cloud shadows and to generate a scene classification map. Please note that this map does not constitute a land cover classification map in a strict sense, its main purpose is to be used internally in Sen2Cor in the atmospheric correction module to distinguish between cloudy pixels, clear land pixels and water pixels.

The scene classification map consists of three different classes for clouds (including cirrus), together with six additional classes for shadows, cloud shadows, vegetation, not-vegetated area, water and snow. Three additional classes for No-data, saturated/defective and unclassified pixels are also foreseen. The scene classification map (12 classes) is delivered at 20 m resolution and if set in the L2A_GIPP.xml configuration file also in the 60 m product.

Associated Quality Indicators (QI) for cloud and snow probabilities are additionally provided. These quality indicators provide the probability (0-100%) that the Earth surface is obstructed by clouds or optically thick aerosol respectively that the Earth surface is covered by snow.

Operational constraints have driven the design of this algorithm. The need for several algorithms to first determine if the pixel is cloudy or clear (e.g. atmospheric correction, mosaics) imposes to the cloud detection algorithm to be fast and efficient, limiting the use of CPU-intensive algorithms.

The algorithm uses the reflective properties of scene features to identify the presence or absence of clouds in a scene. The input data for this algorithm is the Level-1C product, i.e. TOA reflectance.

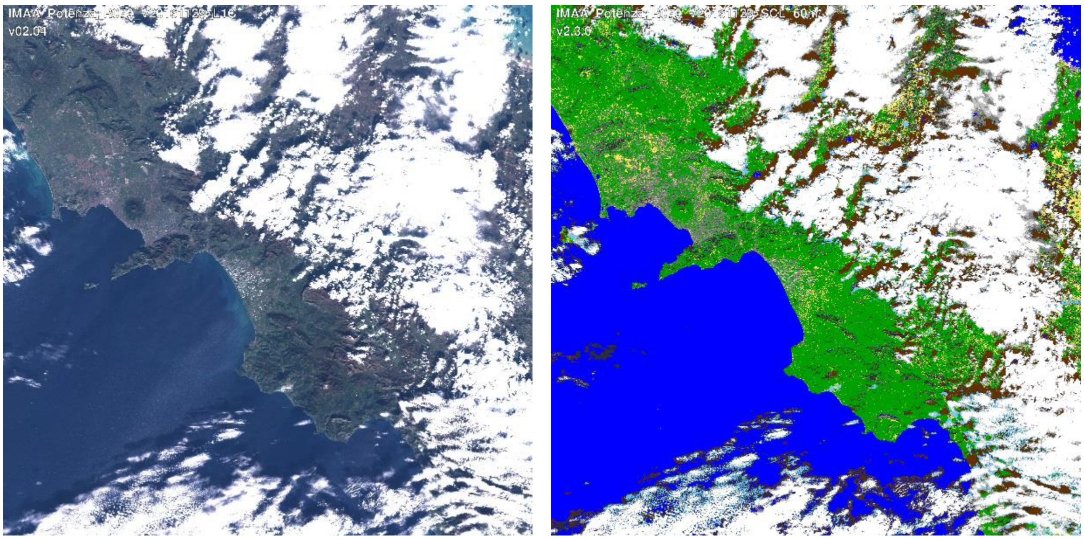

Figure 3-1 – Left L1C image – Right Scene Classification map output

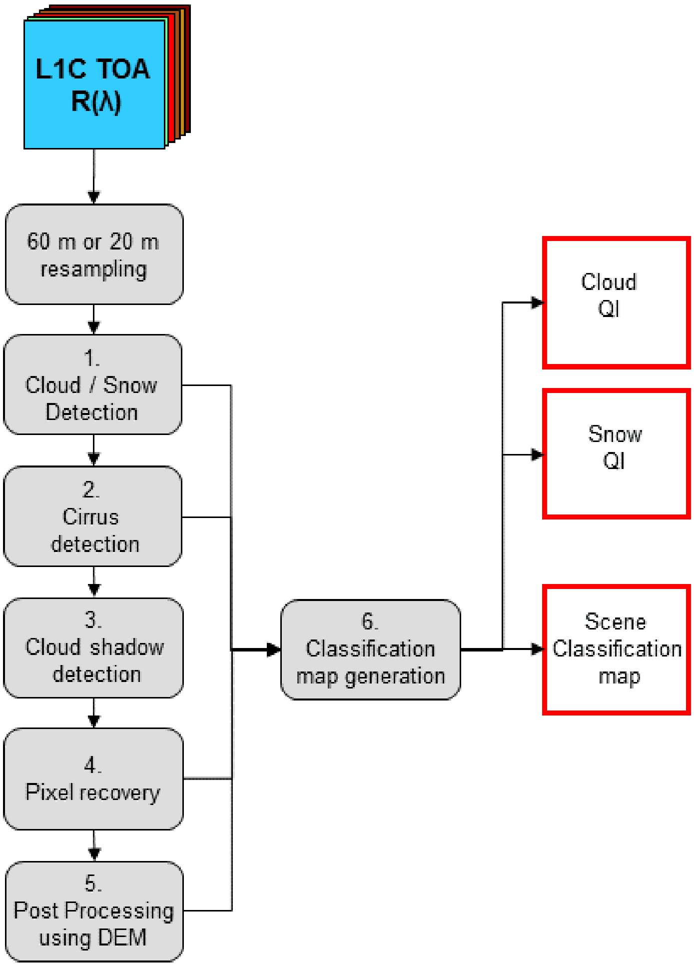

Figure 3-2 – Overview of the processing sequence and outputs

Figure 3-2 gives an overview of the processing sequence of the cloud detection and classification map algorithm. The different processing steps are shown in grey and the final outputs are shown in red.

Each part of the algorithm is described in more details in the following sections:

- The Cloud/Snow detection algorithm is detailed in section 3.2.
- The Cirrus detection algorithm is described in section 3.3.
- The Cloud shadow detection algorithm is presented in section 3.4.
- The Pixel recovery algorithm is detailed in section 3.5.
- The post-processing using DEM information is described in section 3.6.
- The generation of the classification map is presented in section 3.7.

The first pre-processing part of the algorithm is to resample all input bands to the same resolution, e.g. 20 m or 60 m. For the down sampling (10m to 60m) a block_reduce algorithm is used. For the up sampling (60 m to 20 m) a cubic spline is used. It is very important to preserve the geolocation accuracy between bands of different native resolutions as several band ratios are used in this algorithm.

3.2 Cloud/Snow detection algorithm

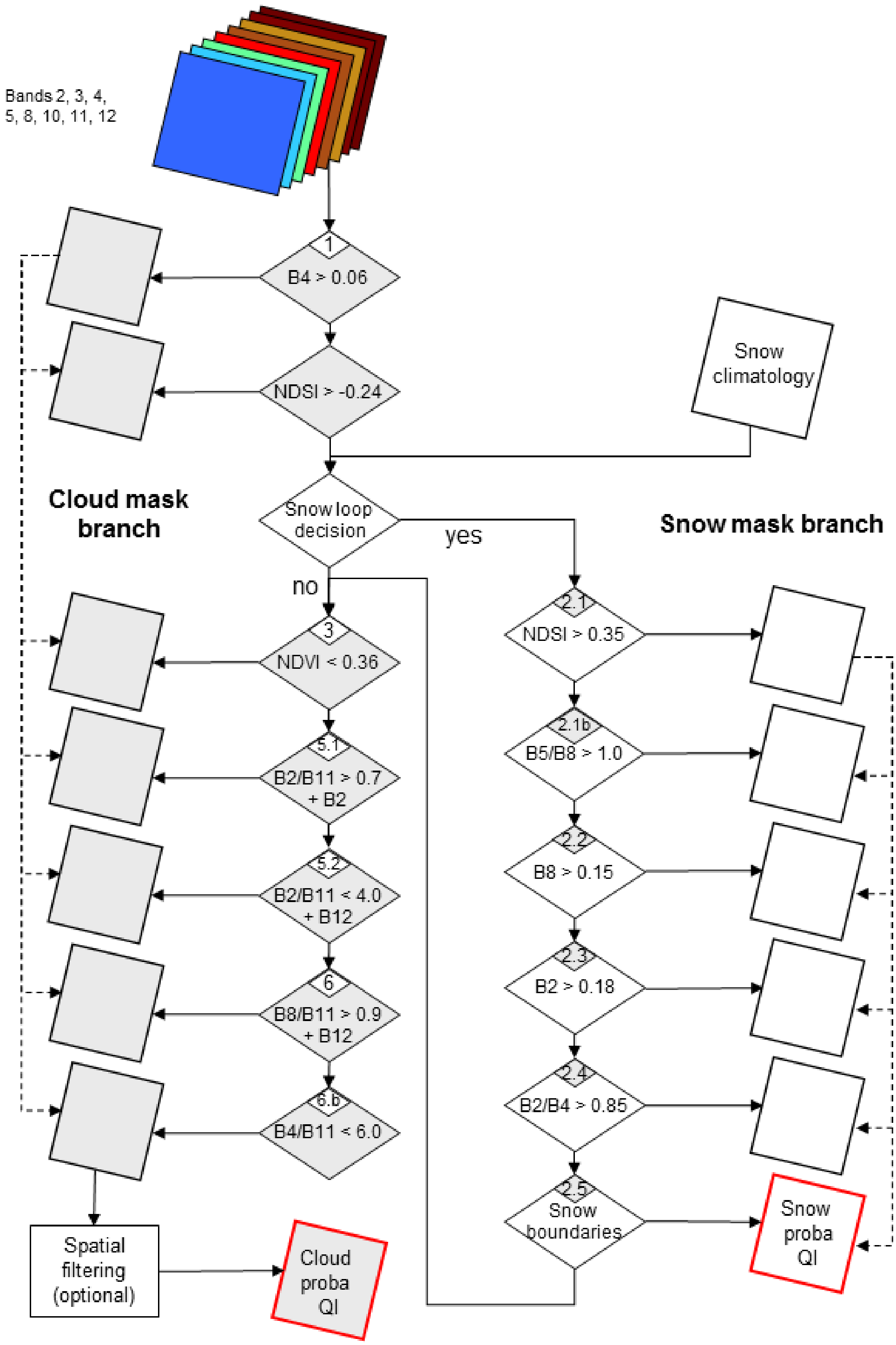

Figure 3-3 – Cloud Detection Algorithm sequential steps

Potential cloudy pixels are identified by a first filtering in the red region of the solar spectrum. Then all these potentially cloudy pixels undergo a sequence of filtering based on spectral bands thresholds, ratios and indexes computations (e.g. NDSI, NDVI). The result of each pixel test is a cloud probability (ranging from 0 for high confidence clear sky to 1 for high confidence cloudy). After each step, the cloud probability of a potentially cloudy pixel is updated by multiplying the current pixel cloud probability by the result of the test. Finally, the cloud probability of a pixel is the "end" product of all the individual tests.

For performance reasons the sequential filtering of a potentially cloudy pixel stops when a test result set its cloud probability to zero. The pixel is then considered to be high confidence clear sky in the cloud probability map and the pixel is finally classified to its corresponding class map shown in Table 3-I.

The Figure 3-3 above presents the sequential steps of the cloud / snow detection module as a flow diagram. Details on the basis for the thresholds values are given by references [7, 8] in Appendix A.

3.2.1 Step 1a - Brightness thresholds on red (Band 4)

The first step of the algorithm is to discard pixels that fall under a certain reflectance threshold in the red region of the solar spectrum.

Each band 4 pixel in the scene is compared to two brightness thresholds. Pixels that fall below the lower brightness threshold have their cloud probability set to 0.0 and are identified as non-clouds and classified as dark pixels in the classification map. Pixels that exceed the upper brightness threshold have their cloud probability set to 1.0 and are passed to step 2. Pixels that have their brightness between these two thresholds have their cloud probability calculated linearly from 0.0 to 1.0 as shown in Figure 3-4 and are passed to step 1b.

Current thresholds (v.2.9.0): T1 = 0.06; T2 = 0.25

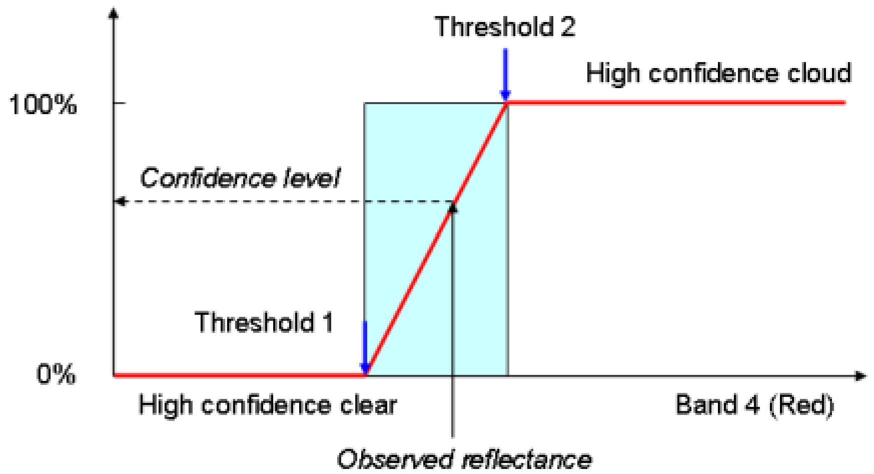

Figure 3-4 – Step 1 confidence level

3.2.2 Step 1b – Normalized Difference Snow Index (NDSI)

Most of potential cloudy pixels have NDSI values located between -0.1 and 0.2 so pixels with strong NDSI negative values could be discarded whereas others continue the algorithm path.

Pixels values from spectral bands 3 and 11 are used to formulate the normalized difference snow index (NDSI). The NDSI filter is expressed as:

NDSI = (band 3 – band 11) / (band 3 + band 11)

Each pixel NDSI value in the scene is compared to two NDSI thresholds. Pixels that fall below the lower NDSI threshold have their cloud probability set to 0.0 and are identified as non-clouds and classified as dark pixels in the classification map. Pixels with NDSI that exceed the upper NDSI threshold have their cloud probability set to 1.0 and are passed to step 2. Pixels that have their NDSI values between these two thresholds have their cloud probability calculated linearly from 0.0 to 1.0 (as shown in Figure 3-5), then multiplied by the precedent cloud probability from step 1a and passed to step 2.

Current thresholds (v2.9.0): T1 = -0.24; T2 = -0.16

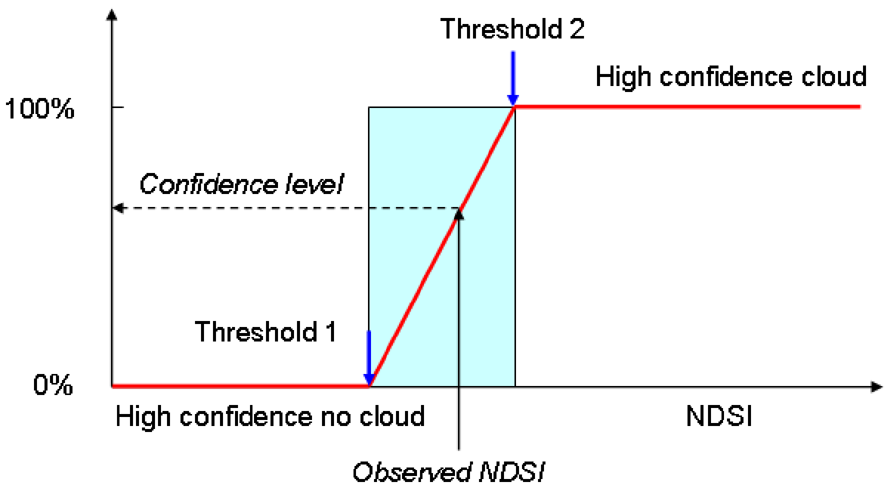

Figure 3-5 – Step 1b confidence level

3.2.3 Step 2 – Snow detection – Snow confidence mask

The objective of this step is to detect snow pixels and to create a snow confidence mask. It consists of four successive filters using pixels values from spectral bands 2, 3, 4, 5, 8a and 11.

The entry into the snow detection branch of the algorithm is conditioned by auxiliary information about snow. A climatology of snow probability is used to trigger the entry into the snow detection loop. This step helps to limit the detection of ice/snow in high altitude, or icy clouds.

Normalized Difference Snow Index (NDSI) computed in step 1a and a successive set of filters and ratios are used to determine the probability that a pixel is covered by snow. The output of the snow detection loop is a snow confidence mask.

An additional processing step is performed in section 3.2.3.8 to limit the cloud false detection around the snow regions boundaries.

3.2.3.1 Snow climatology condition – The entry into snow detection loop

In order to discard false snow detections due to high altitude clouds that behave like snow or ice cover, auxiliary data shall be used in order to determine whether the snow detection algorithm for a particular scene shall be started. For this purpose yearly snow climatology data shall be assembled, which can be derived from the MODIS snow climatology database, putting together a map of the areas where no snow was detected during the years 2000-2010. The spatial resolution of this map is 0.05°. Figure 3-6 and Figure 3-7 show two examples of such no-snow areas in black. This long term no-snow area has to be supplied likewise another auxiliary input data, as described for Table 2-1 in [S2-L2A-PDD].

For each tile, the corresponding tile area of the snow climatology map is read. If this area contains only "no-snow" pixels, then the snow detection loop is discarded and the algorithm continue to the successive cloud detection filters. If at least one climatology pixel appears to have been covered by snow, then the snow detection loop is activated for that whole tile. In the current version 2.9.0, this decision is tile-based, not pixel-based.

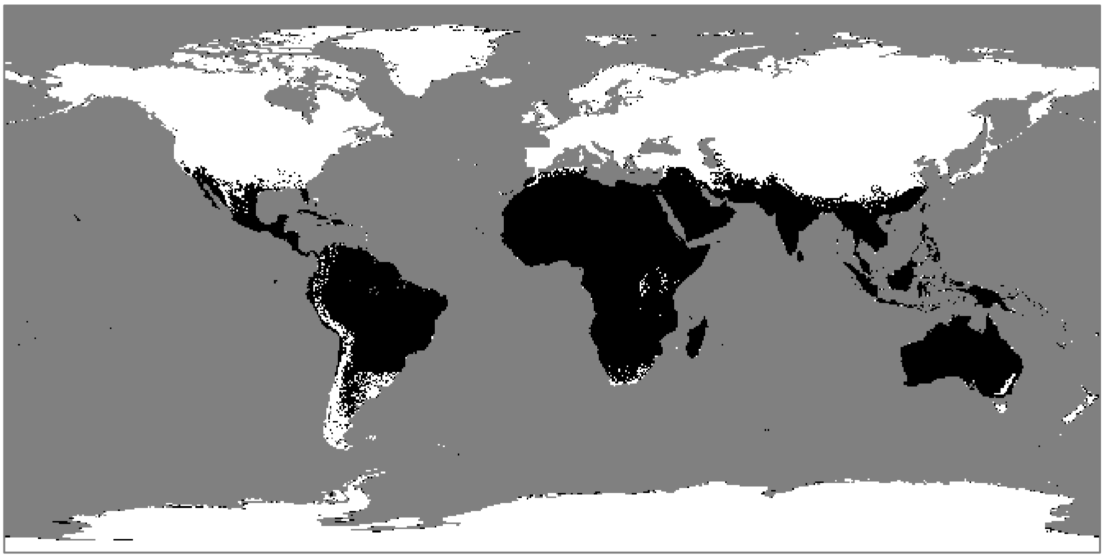

Figure 3-6 – Snow climatology map
(Black = no snow on land during the years 2000-2010) © MODIS

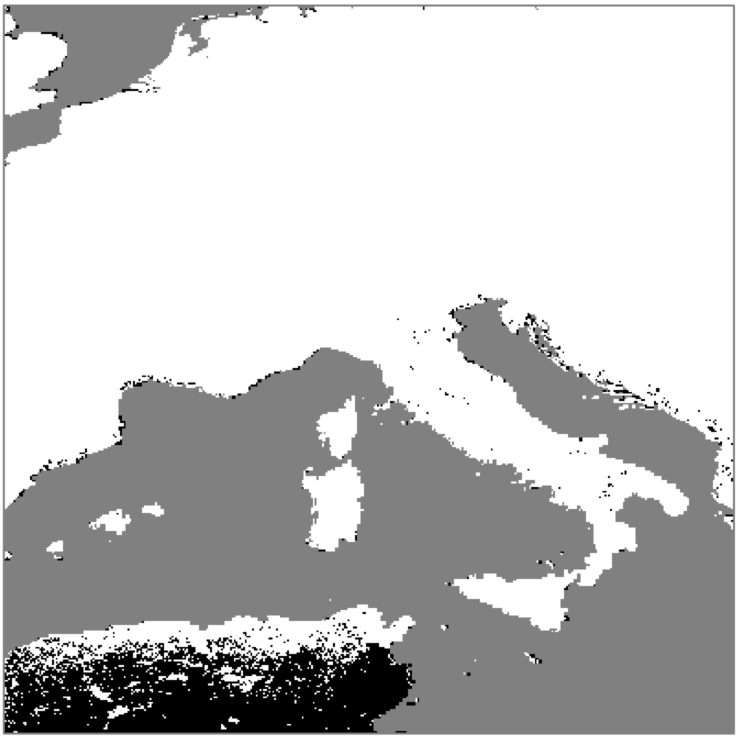

Figure 3-7 – Snow climatology map
zoom over Mediterranean Sea and Italy
(Black = no snow on land during the years 2000-2010) © MODIS

Figure 3-7 is a close-up of Figure 3-6 over Mediterranean Sea and Italy to illustrate that no seldom snow event should be missed over this region due to the use of a snow climatology map.

3.2.3.2 Snow Tri-MONTHLY climatology

With Sen2Cor version 2.10, in order to limit the misclassification of cloud pixels as snow in shaded parts of the clouds or in high altitude icy clouds, a set of 12 "Tri-MONTHLY" Snow condition images has been generated. It is based on a post-processing of the 52 Snow Conditions images from ESA CCI data package, with the objective to identify - for each month of the year - the pixels without any snow occurrence for the period 2000-2010 with +/- one month margin.

These 12 "Tri-MONTHLY" Snow condition images are used in the Snow detection algorithm instead of native SNow Condition (SNC) weekly files that were not able to catch rare snow events or snow/ice on inland waters or icebergs.

Figure 3-8 and Figure 3-9 show examples of snow occurrence on land. The meaning of black colour is that no snow was observed and light grey that snow occurrence is probable. On water, the meaning of light grey is that icebergs could be observed whereas white indicates that snow will not be detected in Sen2Cor.

Figure 3-8 – Snow Monthly Climatology - January

Figure 3-9 – Snow Monthly Climatology - July

Figure 3-10 shows a RGB colour composite of a partly cloudy region of San José in Costa Rica. Figure 3-11 shows the related SCL output of sen2cor v.2.8 where pink colour in the middle/top of convective clouds corresponds to a false snow classification. Finally, the Figure 3-12 shows the related SCL output of sen2cor v.2.10, showing no snow in the middle/top of convective clouds.

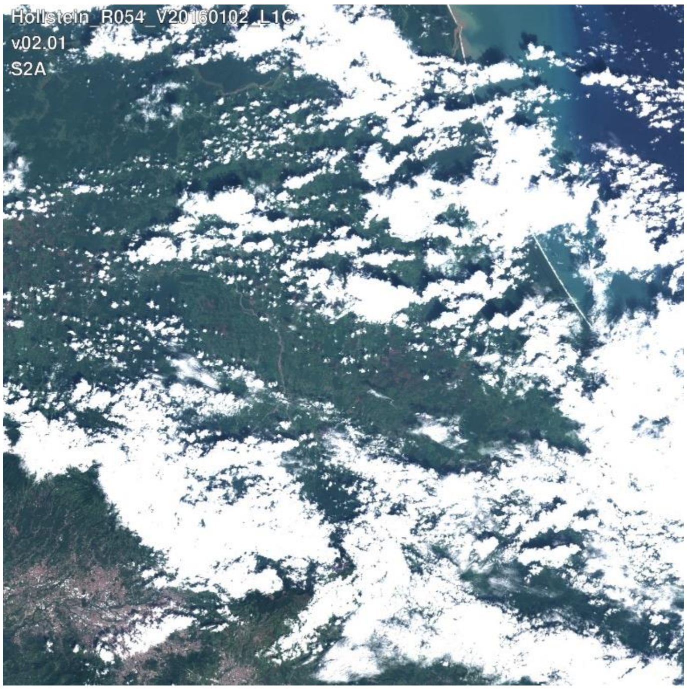

Figure 3-10: Level-1C (RGB) San José, Costa Rica
Tile 16PHS, SZA = 39.7 deg

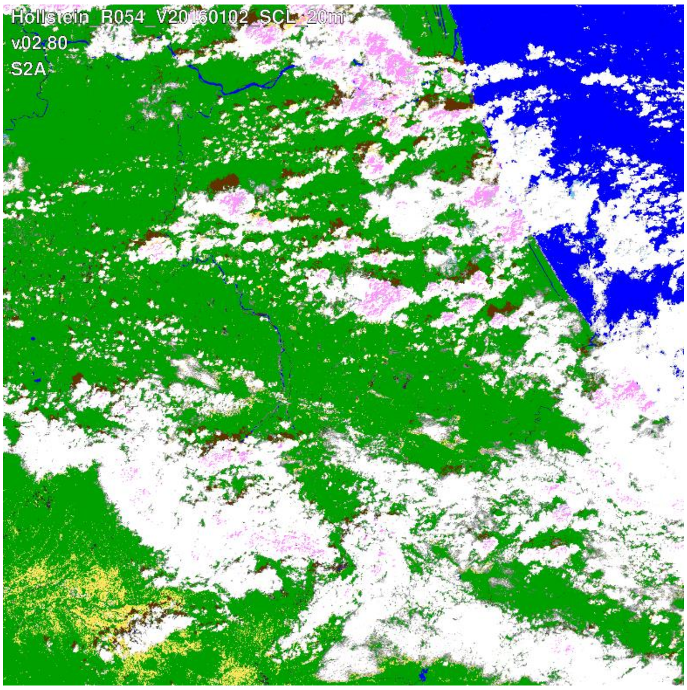

Figure 3-11: SCL Sen2cor 2.8,
San José, Costa Rica, Tile 16PHS, SZA = 39.7 deg

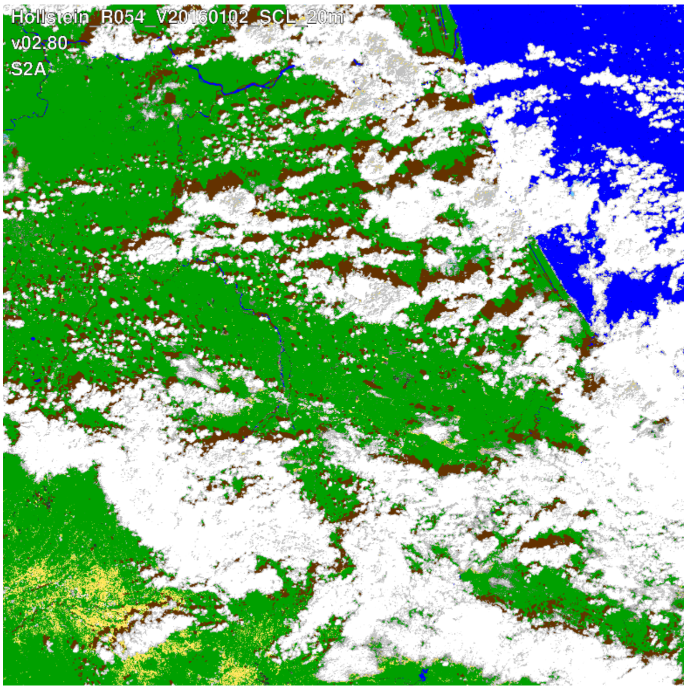

Figure 3-12: SCL Sen2cor 2.10,
San José, Costa Rica, Tile 16PHS, SZA = 39.7 deg

3.2.3.3 Snow filter 1: Normalized Difference Snow Index (NDSI)

Pixels values from spectral bands 3 and 11 are used to formulate the normalized difference snow index (NDSI). The NDSI filter is expressed as:

$$\boxed{\text{NDSI} = (\text{band } 3 - \text{band } 11) \,/\, (\text{band } 3 + \text{band } 11)}$$

This filter is particularly useful for eliminating snow. The reflectance of clouds and snow is similar in band 3. However, in band 11, reflectance for clouds is very high while for snow it is low. NDSI has a long history as described in Hall [9]. Two thresholds are set for the NDSI. NDSI values that fall below the lower threshold have their snow probability set to 0.0 and are identified as non-snow. NDSI values that exceed the upper threshold have their snow probability set to 1.0 and are passed to the snow filter 2. Pixels that have their NDSI between these two thresholds have their snow probability calculated linearly from 0.0 to 1.0 and are passed to snow filter 2.

Current thresholds v2.9.0: T1 = 0.35; T2 = 0.50

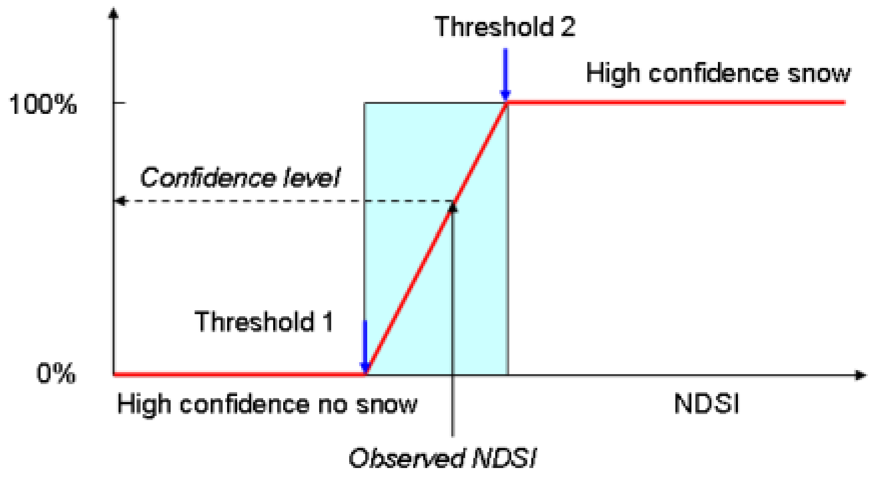

Figure 3-13 – Step 2 – Snow filter 1 confidence level

In addition and only if the usage of ESA CCI maps (Snow Condition (SNC) map and Water Bodies (WBI) map) is activated, following pixels are excluded from the Snow detection algorithm:

a) Pixels identified without snow in weekly SNC.
However this is deactivated since version 2.6.3 because SNC file is not accurate enough to capture for rare events, e.g. Snow in Washington DC 2018 March 22. It is foreseen to reactivate this removal of "without snow" pixels in weekly SNC in a future version but only for Tropical regions: latitude ∊ [-30, 30].

b) Water Pixels from WBI map, if the mean value of SNC for land pixels is higher than 10.0. This condition allows to keep the detection of icebergs that would be discarded if the WBI map is used blindly because WBI does not take into account seasonal ice shelf, e.g. icebergs.
The origin of this exclusion of Water Pixels is to limit the detection of snow/ice in high convective clouds above oceans.

3.2.3.4 Snow filter 1b: Ratio Band 5 / Band 8A

This filter is used to limit false snow detection especially on high altitude clouds. This filter is a single threshold based on snow spectral shape (see Figure 3-14) that shows a systematic decrease of reflectance in the spectral range [705 nm – 865 nm]. Band 5 is centred at 705 nm and Band 8A is centred at 865 nm.

All pixels which ratio (band 5 / band 8A) is higher than 1.0 have their snow probability set to 0 and are identified as non-snow.

Current thresholds v2.9.0: T2_SNOW_R_B05_B8A = 0.85

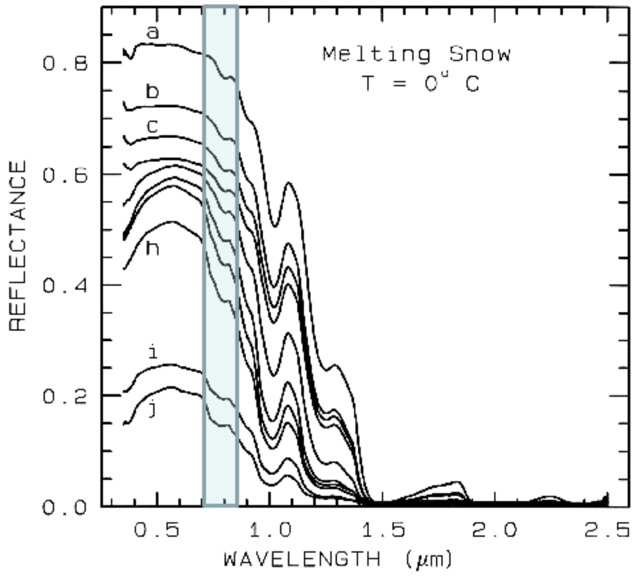

Figure 3-14 – A series of reflectance spectra of melting snow. The top curve (a) is at 0°C and has only a small amount of liquid water, whereas the lowest spectrum (j) is of a puddle of about 3 cm of water on top of the snow. Modified from Clark et al (USGS)1999

3.2.3.5 Snow filter 2: Band 8a thresholds

This filter eliminates regions that have high NDSI values but low reflectance in Band 8a (Near Infrared).

Band 8a pixel values are compared to two brightness thresholds. Pixels that fall below the lower threshold have their snow probability set to 0.0 and are identified as non-snow. Pixel values that exceed the upper threshold have their snow probability that remains unchanged and are passed to the snow filter 3. For pixels that have a value between these two thresholds, a snow probability is computed linearly from 0.0 to 1.0 and multiplied by their precedent snow probability. This new snow probability is stored in the snow confidence mask. These pixels are passed to the snow filter 3.

Current thresholds v2.9.0: T1 = 0.15; T2 = 0.35

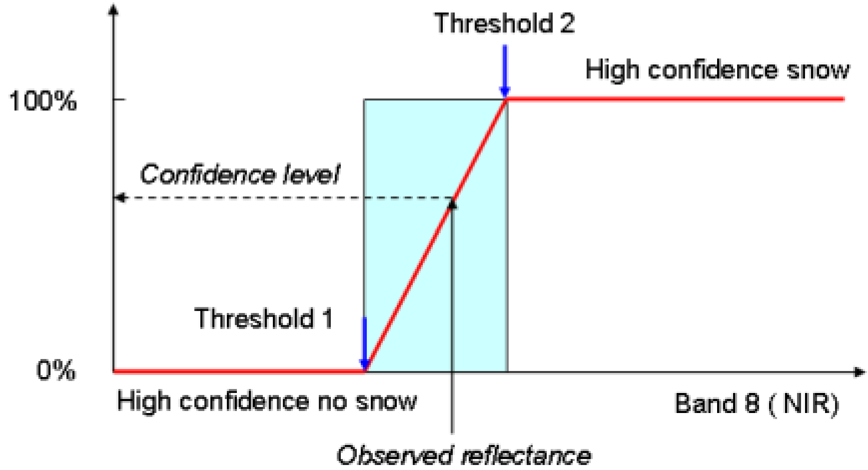

Figure 3-15 – Step 2 – Snow filter 2 confidence level

3.2.3.6 Snow filter 3: Band 2 thresholds

This filter eliminates regions that have high NDSI values but low reflectance in Band 2 (Blue).

Band 2 pixel values are compared to two brightness thresholds. Pixels that fall below the lower threshold have their snow probability set to 0.0 and are identified as non-snow. Pixel values that exceed the upper threshold have their snow probability that remains unchanged and are passed to snow filter 4. For pixels that have a value between these two thresholds, a snow probability is computed linearly from 0.0 to 1.0 and multiplied by their precedent snow probability. This new snow probability is stored in the snow confidence mask. These pixels are passed to the snow filter 4.

Current thresholds v2.9.0: T1 = 0.18; T2 = 0.22

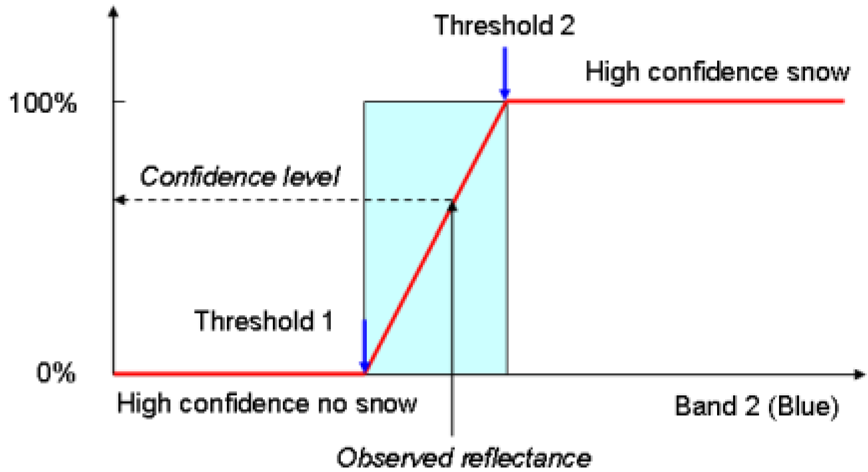

Figure 3-16 – Step 2 – Snow filter 3 confidence levels

3.2.3.7 Snow filter 4: Ratio Band 2 / Band 4

This filter eliminates regions that have high NDSI values but low B2/B4 ratio like some water bodies.

Two thresholds are set for the B2/B4 ratio. B2/B4 ratio values that fall below the lower threshold have their snow probability set to 0.0 and are identified as non-snow. B2/B4 ratio values that exceed the upper threshold have their snow confidence that remain unchanged and are passed to the following step. For pixels that have a B2/B4 ratio between these two thresholds, a probability is computed linearly from 0.0 to 1.0 and multiplied by their precedent snow probability. This new snow probability is stored in the snow confidence mask.

All the pixels that have a snow confidence value higher than 0 are passed to the step 5.

Current thresholds v2.9.0: T1 = 0.85; T2 = 0.95

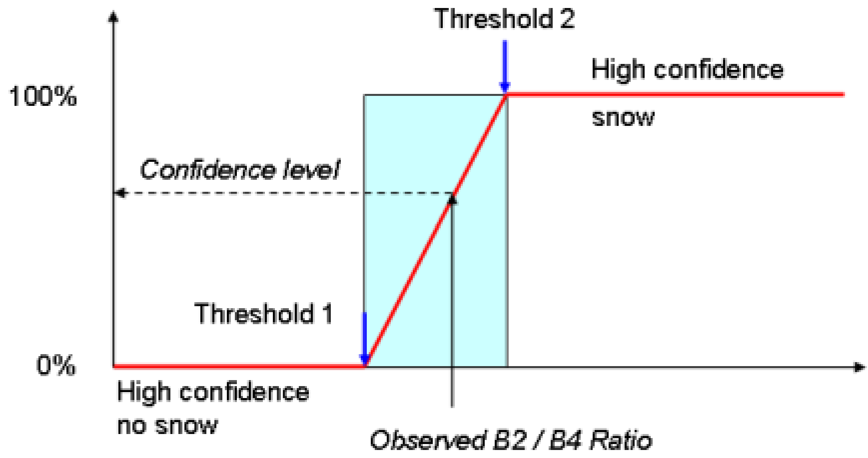

Figure 3-17 – Snow filter 4 confidence levels

3.2.3.8 Snow filter 5: Processing of snow boundaries zones

This step helps to remove false cloud detection at the boundaries of a snowy region, where mixed pixel (snow + ground) could be detected as cloud in the cloud detection algorithm.

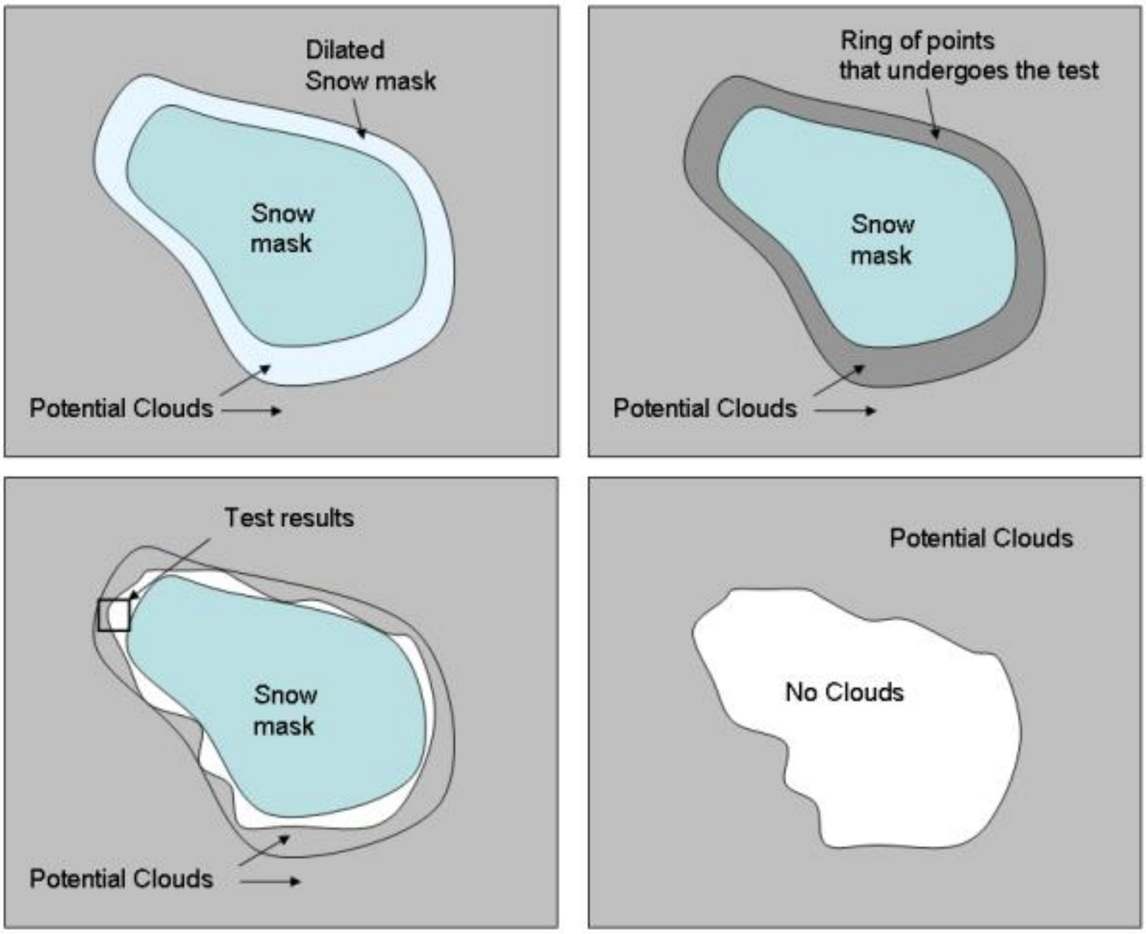

Figure 3-18 – Snow boundary region filtering

A "DILATE[3]" operator is used to determine a boundary zone (ring of pixels around a snowy region) on which a brightness test on Band 12 is performed.

Pixel values of band 12 that fall below a threshold of T2_SNOW = 0.25 have their snow confidence that remain unchanged. Pixels that exceed the threshold have their snow probability set to 0.0 and are identified as non-snow.

The result of this processing step is to extend the detected snow mask in a controlled manner to avoid cloud over-detection on partially snowy pixels.

3.2.3.9 Snow detection post processing

This step occurs only if the usage of ESA CCI maps (Snow Condition (SNC) map and Water Bodies (WBI) map) is activated. A check is performed on the snow boundary zone pixels to verify if they are no snow pixels from SNC map or water pixels in WBI. See end of section 3.2.3.3 Snow filter 1 for details of check.

[3] Dilation is a mathematical morphology method in order to gradually enlarge the boundaries of regions of foreground pixels. Areas of foreground pixels grow in size while holes within those regions become smaller.

3.2.3.10 End of snow detection loop

The pixels that have a snow probability that fall below a threshold of T1_SNOW = 0.12 are passed to the next cloud detection step whereas pixels that have their snow probability higher than this threshold are classified as snowy pixels in the classification map.

3.2.4 Step 3 – Normalized Difference Vegetation Index (NDVI)

This filter based on the Normalized Difference Vegetation Index (NDVI) is used to identify vegetation pixel. Please note that it is an approximation as this NDVI is computed using TOA reflectances instead of surface reflectances.

Pixel values from spectral bands 8a and 4 are used to formulate the normalized vegetation index (NDVI). The NDVI filter is expressed as:

$$\boxed{NDVI = (band\ 8a - band\ 4) / (band\ 8a + band4)}$$

This filter is particularly useful for eliminating highly reflective vegetation. In the near-infrared (band 8a), reflectance for green leaves is high because very little energy is absorbed. In the red region (band 4), the chlorophyll in green leaves absorbs energy so reflectance is low. The NDVI results in higher values for vegetation than for other scene features, including clouds. Two thresholds are set for the NDVI. NDVI values that exceed the upper threshold have their cloud probability set to 0.0 and are identified as non-cloud. An additional condition is necessary for those high NDVI pixels to be classified as vegetation in the classification map: their reflectance in blue band B2 shall be below T1_B2T = 0.15.

NDVI values that fall below the lower threshold have their cloud confidence that remain unchanged and are passed to the fourth step. For pixels that have a NDVI value between these two thresholds, a probability is computed linearly from 1.0 to 0.0 and multiplied by their precedent cloud probability. This new cloud probability is stored in the cloud confidence mask.

Current thresholds v2.9.0: T1 = 0.36; T2 = 0.42

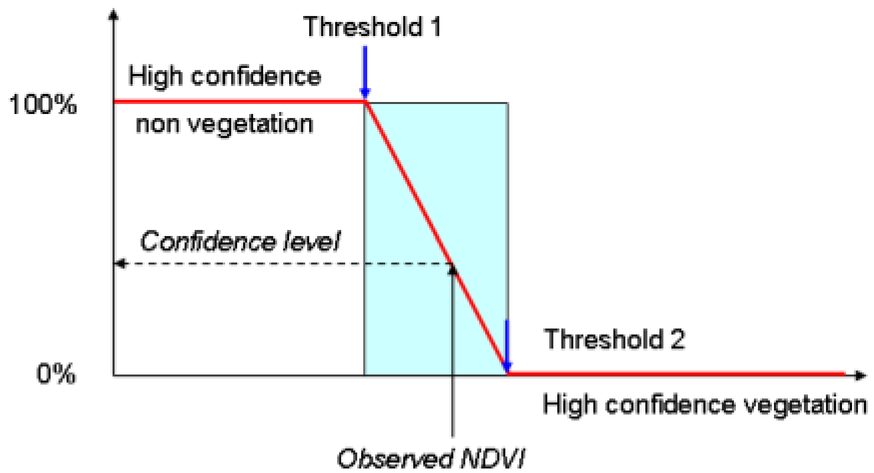

Figure 3-19 – Step 3 confidence level

All the pixels that have a cloud confidence value higher than 0 are passed to the step 4.

3.2.5 Step 4 – Ratio Band 8 / Band 3 for senescing vegetation (disabled)

This filter is disabled since Sen2Cor v2.3.1.

3.2.6 Step 5 – Ratio Band 2 / Band 11 for not-vegetated pixels and water bodies

Not-vegetated pixels (e.g. bare soils, impervious ground) are detected when their reflectance ratio (blue/infrared, B2/B11) fall below a threshold. An additional variable offset threshold in the infrared region (B12) is added to detect thin cloud over soils.

Bright waters pixels are identified when their reflectance ratio (blue/infrared, B2/B11) exceed a threshold. An additional variable offset threshold in the blue region is added to detect thin cloud over inland waters.

3.2.6.1 Step 5.1 (pass 1) for not-vegetated pixels detection

The pass1 eliminates different types of not-vegetated pixels. It is formed by dividing the reflectance of band 2 by the reflectance of band 11. The B2/B11 ratio values are lower for not-vegetated (e.g. soils) than other scene features including clouds.

The entry into this test is conditioned by threshold on pixel value in Band 2. The pixel enters the test only if its value in Band 2 is lower than a threshold (B02_FT between 0.15 and 0.32) that varies linearly in function of B2/B11 ratio. The lower is the B2/B11 ratio (higher probability to be a not-vegetated pixel) the lower is the threshold to enter the test and vice versa. It helps to keep thin clouds detection over soil regions.

For the pass 1, two thresholds are set for the B2/B11 ratio. B2/B11 ratio values that fall below the lower threshold have their cloud probability set to 0.0 and are identified as non-cloud and classified as not-vegetated pixels in the classification map. B2/B11 ratio values that exceed the upper threshold have their cloud confidence that remain unchanged and are passed to the step 5 pass 2. For pixels that have a B2/B11 ratio between these two thresholds, their precedent cloud probability is multiplied by a probability computed linearly from 0.0 to 1.0. This new cloud probability is stored in the cloud confidence mask. These pixels are passed to the step 5 pass 2.

3.2.6.2 Step 5.2 (pass 2) for water bodies detection

This filter pass 2 eliminates different types of water bodies and is formed by dividing the band 2 reflectance by the band 11 reflectance. The B2/B11 ratio values are higher for water bodies than other scene features including clouds.

The entry into this test is conditioned by threshold on pixel value in Band 12. The pixel enters the test only if its value in Band 12 is lower than a threshold that varies linearly in function of B2/B11 ratio. The higher is the B2/B11 ratio (higher probability to be a water body pixel) the higher is the threshold to enter the test and vice versa. It helps to keep thin clouds detection over some water regions.

Two thresholds are set for the B2/B11 ratio pass 2. B2/B11 ratio values that exceed the upper threshold have their cloud probability set to 0.0 and are identified as non-cloud. There are additional conditions necessary for those high B2/B11 ratio pixels to be classified as water in the classification map: their reflectance in blue band B2 shall be below T_B02 = 0.2 and the reflectance in the NIR (B8A) shall be less than the reflectance in the red (B4). B2/B11 ratio values that fall below the lower threshold have their cloud confidence that remain unchanged and are passed to the step 6. For pixels that have a B2/B11 ratio between these two thresholds, their precedent cloud probability is multiplied by a probability computed linearly from 0.0 to 1.0. This new cloud probability is stored in the cloud confidence mask.

All the pixels that have a cloud confidence value higher than 0 are passed to the step 6.

Current thresholds v2.9.0: T11 = 0.70; T12 = 1.0; T21 = 2.0; T22 = 4.0

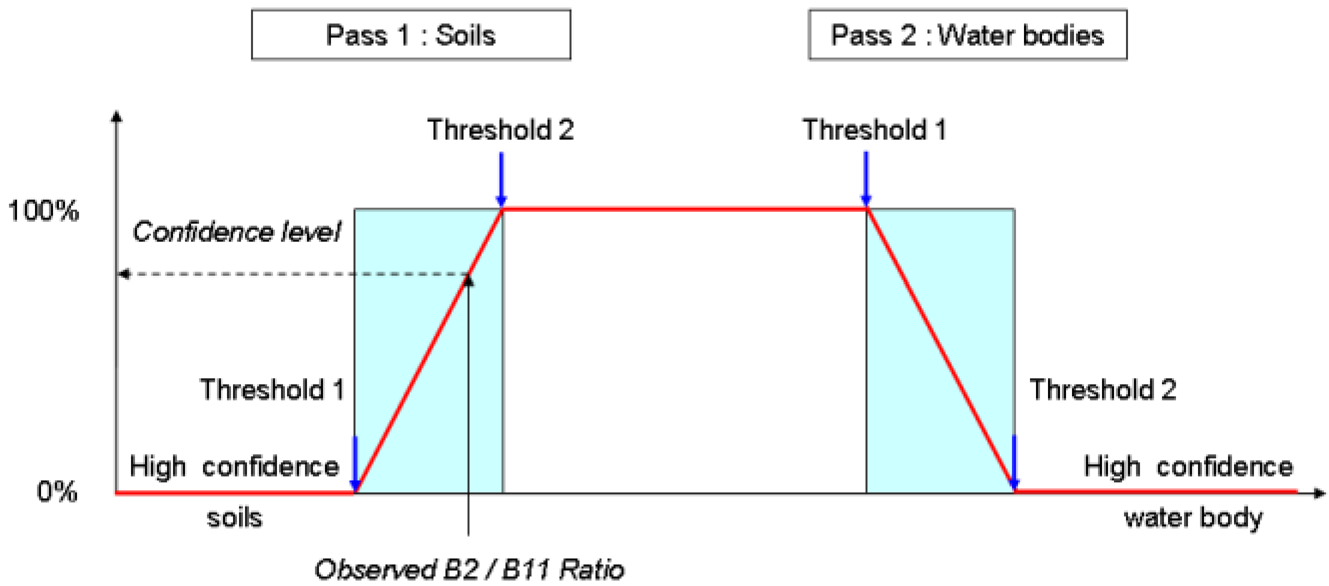

Figure 3-20 – Step 5 – Pass 1 & Pass 2 confidence level

An additional check is applied on all unclassified pixels to verify if some water pixels were missed. The conditions are that: the surface reflectance difference between Band 2 and Band 4 shall be higher than T_24 = 0.034 (i.e. B2-B4 > T_24) and the reflectance in the NIR (B8A) shall be less than the reflectance in the red (B4) and their reflectance in blue band B2 shall be below T_B02 = 0.2.

3.2.7 Step 6 – Ratio Band 8 / band 11 for rocks and sands in deserts (not-vegetated)

This filter eliminates highly reflective rocks and sands in desert landscapes and is formed by dividing the band 8 reflectance by the band 11 reflectance. Rocks and sand tend to exhibit higher reflectance in band 11 than in band 8, whereas the reverse is true for clouds.

The entry into this test is conditioned by threshold on pixel value in Band 2. The pixel enters the test only if its value in Band 2 is lower than a threshold (B02_FT between 0.16 and 0.32) that varies linearly in function of B8/B11 ratio. The lower is the B8/B11 ratio (higher probability to be a not-vegetated pixel) the lower is the threshold to enter the test and vice versa. It helps to keep thin clouds detection over desert regions.

Two thresholds are set for the B8/B11 ratio. B8/B11 ratio values that fall below the lower threshold have their cloud probability set to 0.0 and are identified as non-cloud. There are additional conditions necessary for those low B8/B11 ratio pixels to be classified as not-vegetated in the classification map: their reflectance in blue band B2 shall less than 80% of their reflectance in B11.

B8/B11 ratio values that exceed the upper threshold have their cloud confidence that remain unchanged and are passed to step 7. For pixels that have a B8/B11 ratio between these two thresholds, a probability is computed linearly from 0.0 to 1.0 and multiplied by their precedent cloud probability. This new cloud probability is stored in the cloud confidence mask.

All the pixels that have a cloud confidence value higher than 0 are passed to the step 7.

Current thresholds v2.9.0 : T1 = 0.90; T2 = 1.10

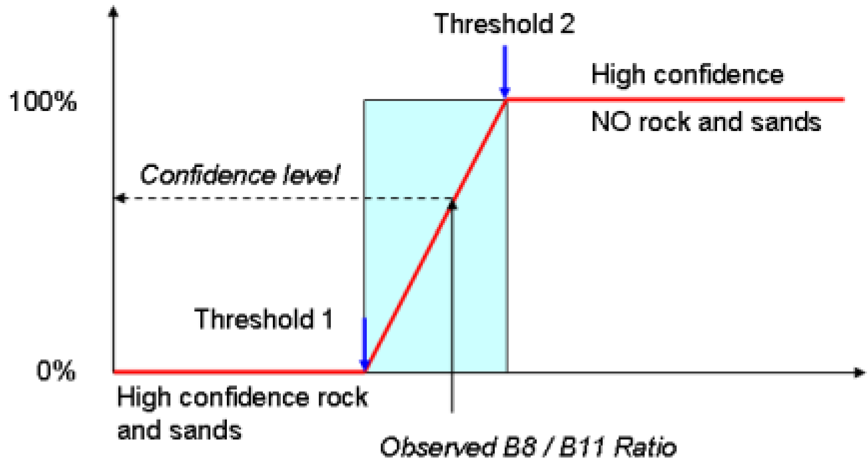

Figure 3-21 – Step 6 confidence level

3.2.8 Step 6bis – Ratio Band 4 / band 11

This filter eliminates potential cloud pixels with very high ratio B4/B11. It is formed by dividing the band 4 reflectance by the band 11 reflectance.

Two thresholds are set for the B4/B11 ratio. B4/B11 ratio values that exceed the upper threshold have their cloud probability set to 0.0 and are identified as non-cloud.

B4/B11 ratio values that fall lower below the lower threshold have their cloud confidence that remain unchanged and are passed to step 7. For pixels that have a B8/B11 ratio between these two thresholds, a probability is computed linearly from 0.0 to 1.0 and multiplied by their precedent cloud probability. This new cloud probability is stored in the cloud confidence mask.

All the pixels that have a cloud confidence value higher than 0 are passed to the step 7.

Current thresholds v2.9.0 : T1 = 3.0; T2 = 6.0

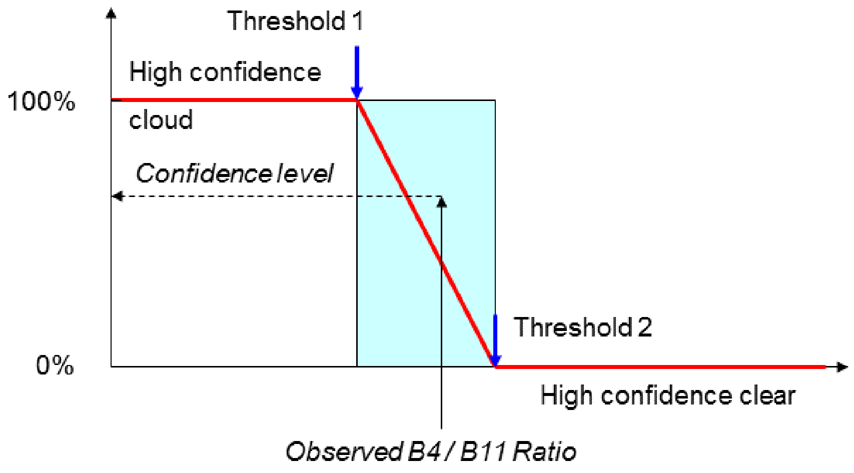

Figure 3-22 – Step 6 confidence level

3.2.9 Step 7 – Spatial filtering

At this stage of the algorithm a cloud confidence mask and a snow confidence mask are available.

An optional spatial filtering is proposed to take into account the slight misregistration of S2 spectral bands at the altitude of clouds. Indeed S2 spectral bands are co-registered at ground level with the use of a digital elevation model. The spatial filtering helps also to reduce false cloud detection that occurs on the borders of highly contrasted regions like river contours or shorelines.

It consists in applying a median filter[4] followed by a dilatation[5] operator to the final cloud mask. The kernel size of the filters could be set to 3x3 or 5x5 depending on the level of artefacts reduction desired.

This spatial filtering is done for the generation of the two cloud classes and the thin cirrus class in the classification map.

Only the option of median filtering is available in Sen2Cor v2.9.0 (not activated by default).

Note: Please keep in mind that Sen2Cor cloud mask can be considered as a "raw" pixel-based cloud mask that can be further processed by users depending on their particular application. Users who privilege very clean pixels would need a more conservative cloud mask and can dilate Sen2Cor cloud mask. One reason why Sen2Cor cloud mask is not provided already dilated is because the dilatation

[4] The median filter compares each pixel with its nearby neighbours in order to decide whether or not it is representative of its surroundings. Instead of simply replacing the pixel value with the *mean* of neighbouring pixel values, it replaces it with the *median* of those values. The median is a more robust average than the mean so that single very unrepresentative pixels will not affect the resulting value significantly.

[5] See Footnote 2 for explanation.

process of the cloud mask is not reversible and in some cases, users may be interested in getting as much information as possible from their data. They can then use the original Sen2Cor cloud mask for their processing.

3.3 Cirrus cloud detection algorithm

3.3.1 Sentinel-2 band 10 (1.38 µm) thresholds

Cirrus cloud detection relies on **Sentinel-2 band 10 (1.375 µm)** reflectance thresholds on a per pixel basis to detect the presence of thin cirrus cloud in the upper troposphere under daytime viewing conditions.

The strength of this cloud detection band lies in the strong water vapour absorption in the 1.38 µm region (Gao et al., 1993). With sufficient atmospheric water vapour present (estimated to be about 1 cm precipitable water) in the beam path, no upwelling reflected radiance from the earth’s surface reaches the satellite. This means that much of the earth’s surface will be obscured in this band. (However this is not true for the entire earth’s surface because precipitable water is often less than 1 cm over polar regions, in midlatitude winter regions, and in high elevation regions).

With relatively little of the atmosphere’s moisture located high in the troposphere, high clouds appear bright in the S2 Band 10. Reflectance from low and mid level clouds is partially attenuated by water vapour absorption.

Simple low and high reflectance (normalized by incoming solar radiation at the top of the atmosphere) thresholds are used to separate thin cirrus from clear sky and thick clouds. If the reflectance exceeds the clear-sky threshold and is below the thick cloud threshold, then thin cirrus are detected. We subjectively define thin cirrus as a cloud that has a small impact on the visible reflectance, enabling atmospheric correction to be applied to retrieve land surface properties. Two reflectance thresholds have been determined for band 10 to identify thin cirrus:

Current thresholds: T1 = 0.012; T2 = 0.035

An additional threshold for cirrus is applied on Band 2 with a maximum reflectance in the blue band equal to 0.50.

All pixels that have a value in between the two B10 given ranges and below 0.5 in the blue are classified as thin cirrus in the first step.

3.3.2 Cross check with cloud quality indicator

An additional cross check is done with the probabilistic cloud mask obtained by the cloud detection algorithm described previously. This is due to the fact that pixels classified to be cirrus can have a cloud probability higher than 0. The cloud probability of thin cirrus cloud pixels detected by S2 Band 10 is checked:

- If the cloud probability is above 0.80 then the thin cirrus cloud classification is rejected and the pixel classification is set to Cloud high probability.

- If the cloud probability is above 0.20 then the thin cirrus cloud classification is rejected and the pixel classification is set to Cloud medium probability.

- If the cloud probability is below or equal 0.20 then the thin cirrus cloud classification is accepted.

3.3.3 Restrictions

Ben-Dor (1994) analyzed a scene from the AVIRIS to demonstrate that thin cirrus detection using 1.38 µm observations may be more difficult for elevated surfaces (>2000m), dry atmospheric conditions, and high albedo surfaces. New injections of volcanic aerosols into the stratosphere may also impact this test.

It is the reason why, if a DEM is present, the elevation information is used to disable cirrus detection above elevations higher than 1500m, in order to avoid false cirrus detection instead of snow detection.

3.4 Cloud Shadow detection algorithm

The cloud shadow mask is constructed using "geometrically probable" cloud shadows derived from the final cloud mask, sun position and cloud height distribution and "radiometrically probable" cloud shadow derived from the radiometric properties of the pixels.

The literature shows that it is difficult to derive clouds shadow based only on radiometric behaviour because natural features like lakes or hill shadows can present the same spectral signature as cloud shadows. On the other hand it is also time consuming to search geometrically and iteratively for cloud shadow without a good a-priori estimation of the top-cloud height. Therefore the method we propose here is a combination of these two methods, radiometric and geometric.

3.4.1 Radiometric input

The radiometric input is obtained by identifying potential cloud shadows or "dark areas" based on a reference shadow spectral shape defined with bands B2, B3, B4, B8A, B11, B12. This reference dark spectrum was built from a large range of cloud shadows examples on different type of land covers. Some spectral examples are shown in Figure 3-23.

Pixels with a spectrum close or darker than the reference shadow spectral shape are considered as potential cloud shadows.

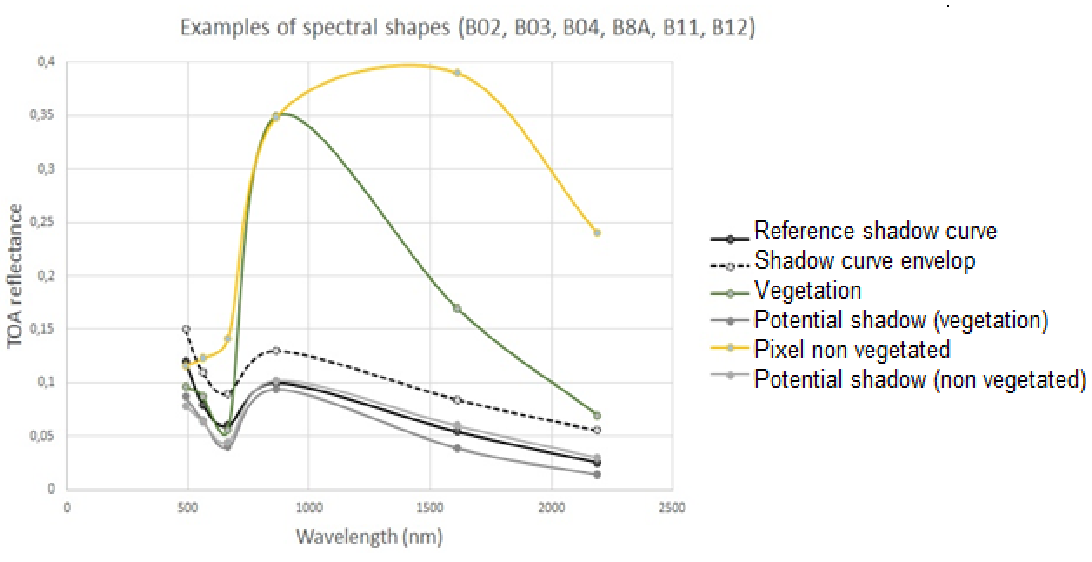

Figure 3-23 – Examples of pixel spectral shapes based on bands B02, B03, B04, B8A, B11, B12. Black curve represents the reference cloud shadow spectrum. The dashed curve (+0.03) represents an upper limit. Examples for vegetation and not-vegetated pixels spectra, under clear sky and cloud shadow conditions are shown.

Since Sen2Cor version 2.10, the cloud shadow algorithm has been enhanced to catch cloud shadows on brighter surfaces using a varying spectral definition of the cloud shadow radiometry.

3.4.2 Geometric input

The geometric input, a mask of "geometrically probable" cloud shadows, is derived from the final cloud mask obtained previously. It helps to resolve any ambiguity about "false cloud shadows" like lakes, dark areas or hill shadows from the first radiometric classification of shadows.

The mask uses the position of the sun, sun elevation, azimuth angles, and an empirical model for top-cloud height distribution shown on Figure 3-24. This empirical distribution has been derived from the analysis the Goddard/Irish cloud assessment dataset [10], studying the statistics on clouds mask, projected cloud shadows distance and solar configuration. The mask of "geometrically" probable cloud shadows has the same resolution as the final cloud mask (20m or 60m) and gives a probability of cloud shadow that depends on the distance of projection of the cloud shadow.

Since Sen2Cor version 2.10 the top-cloud height distribution is derived from statistics of the image itself using the parallax properties of the Sentinel-2 MSI instrument as detailed in section.

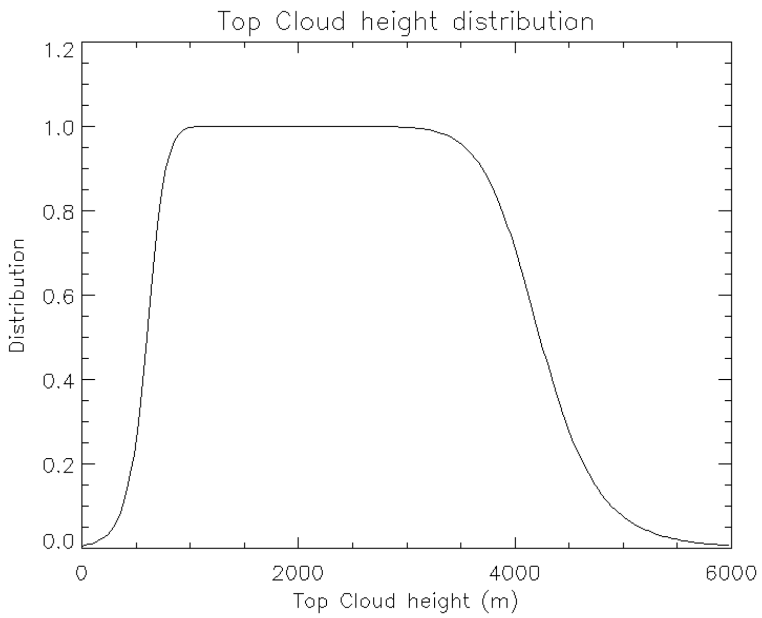

Figure 3-24 – Empirical Top-Cloud height distribution

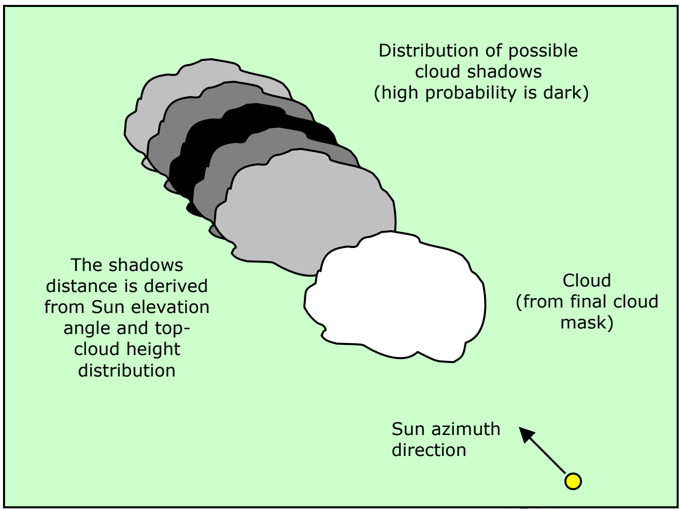

Figure 3-25 – Schematic illustration of the distribution of probable cloud shadows

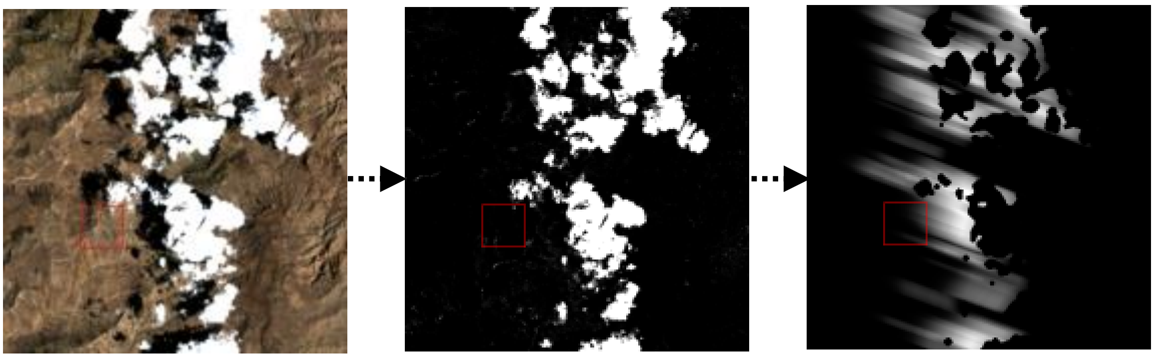

Figure 3-26 – Mask of "geometrically" probable cloud shadows

The computation of this mask is done by the convolution of the final cloud mask by a kernel describing the distribution of "geometrically" probable cloud shadows projected on the ground (assumed to be flat).

3.4.3 Generation of cloud shadow mask

The sequence of processing steps to generate the final cloud shadow mask is shown in Figure 3-27. The final cloud shadow mask is obtained by multiplying the result of the radiometric branch by the result of the geometric branch.

3.4.4 Adding cloud shadow information to the classification map

The pixels that have a cloud shadow probability that exceed a threshold are classified as cloud shadows pixels in the classification map.

3.4.5 Restrictions

This cloud shadow detection algorithm is not suitable to detect cloud shadows over water bodies. The cloud shadows over water are expected to be classified as water bodies in the classification map.

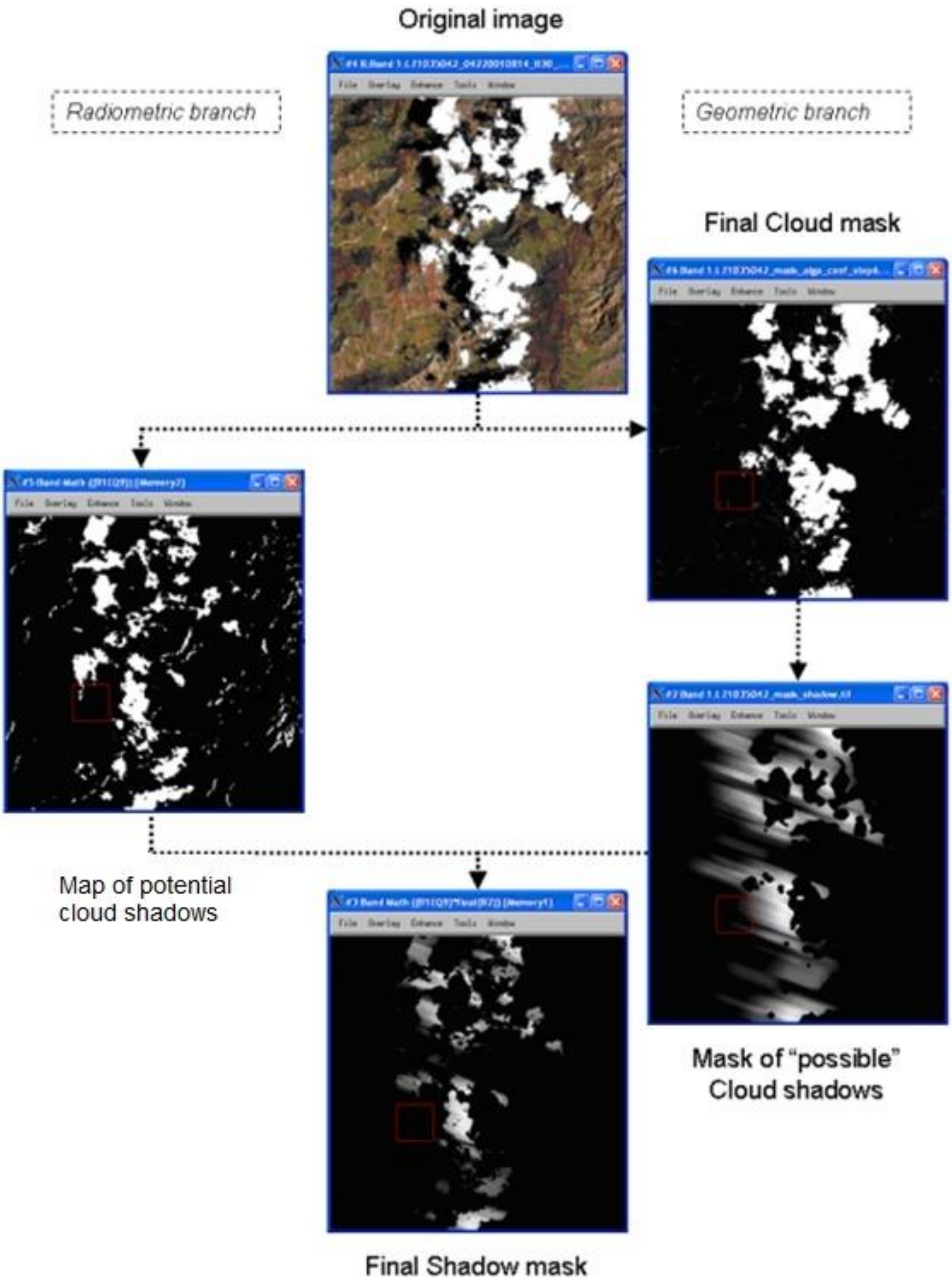

Figure 3-27 – Schematic view of the algorithm for cloud shadow mask generation

3.5 Pixel recovery algorithm

The scope of this step is to test if pixels initially classified as "dark_features" in step 1a (see section 3.2.1), could be reclassified as vegetation or water pixels.

3.5.1 Dark Vegetation pixels recovery

The scope of this step is to test if pixels initially classified as "dark_features" in step 1a, could be reclassified as vegetation pixels by applying to them the threshold test of step 3 (see section 3.2.4).

3.5.2 Water pixels recovery

3.5.2.1 Standard:

The scope of this step is to test if pixels initially classified as "dark_features" in step 1a, could be reclassified as water pixels by applying to them the same thresholds described in step 5 pass2 (see section 3.2.6).

3.5.2.2 With ESA CCI Water Bodies Map:

If the usage of ESA CCI Water Bodies (WBI) map is activated, then the pixels initially classified as "dark_features", "cloud_shadows", "not_classified", could be reclassified as water pixels if those pixels belong to water class in the WBI map.

3.5.3 Snow pixels recovery

The scope of this step is to test if pixels still not classified located at the edges of snow patches could be reclassified as "snow or ice" pixels by verifying if reflectance in band 11 is lower than reflectance in Band 3.

Please note that this "snow pixels recovery" step is performed only after the post-processing with DEM information.

3.5.4 Not-vegetated pixels recovery

The scope of this step is to test if pixels initially classified as "dark_features" in step 1a, could be reclassified as "not-vegetated" pixels by applying to them a threshold on the B2/B11 ratio that shall be higher than 0.65.

Please note that this "not-vegetated pixels recovery" step is performed only after the post-processing with DEM information.

3.5.5 Land pixels recovery with B10, B09, B8A

The scope of this step is use the information contained in the water absorption bands (B09 and B10) to improve the cloud detection over land, in particular to limit the false detection of clouds above bright targets like urban buildings or bright soils, without missing true clouds.

It is necessary to have enough Land reference pixels to perform this Land pixel recovery. In this algorithm, the land reference pixels correspond to the union of vegetation class and not-vegetated class of the scene classification algorithm. Two conditions are needed:

- First condition is that the land pixels percentage in the image is higher than 5%.

- Second condition is that the land area is greater than 121 km^2 (11 km x 11 km), i.e. more than 1% of a full Sentinel-2 tile.

3.5.5.1 B10 threshold

This threshold on B10 (T_B10) band is used to reclassify cloudy pixels with very low B10 brightness (close to ground) into not-vegetated pixels without removing true clouds. A minimum B10 threshold on land is set at 0.0015 or 15 in L1C DN.

Three cases are distinguished:

1) High Probability Cloud (HPC) percentage > 20%:

   T_B10_1 = mean (B10 HPC pixels) – 2 * std (B10 HPC pixels)

   T_B10_2 = mean (B10 Land pixels)

   T_B10 = min (T_B10_1, T_B10_2)

2) High Probability Cloud percentage < 2%:

   T_B10 = mean (B10 Land pixels)

3) 2% < High Probability Cloud percentage < 20%:

   Same statistics as for case 1 but only for HP Clouds greater than 300 m x 300 m, i.e. 25 pixels at 60 m resolution.

3.5.5.2 Ratio B09 / B8A threshold

This threshold on the ratio B09/B8A is used reclassify cloudy pixels with low ratio B09/B8A (close to ground) into not-vegetated pixels without removing true clouds.

T_Ratio_B09_B8A = mean (Ratio_B09_B8A Land pixels) + std (Ratio_B09_B8A Land Pixels)

3.5.5.3 Cloudy pixels reclassification into not-vegetated pixels

The ESA CCI Water Bodies (WBI) map is used to perform this reclassification only on land pixels which satisfy the two threshold conditions above.

(B10 < T_B10) & (Ratio_B09_B8A < T_Ratio_B09_B8A)

Please note that this "land pixels recovery" step is performed only after the post-processing with DEM information.

3.5.6 Cirrus pixels recovery with B10

The scope of this step is to catch more cirrus (e.g. thin clouds or cloud border above water) pixels above previously classified land and water pixels using dynamic B10 thresholds.

A minimum B10 threshold on land is set at 0.0030 or 30 in L1C DN.

A minimum B10 threshold on water is set at 0.0020 or 20 in L1C DN.

T2_B10_Land = mean (B10 not-vegetated) + 3 * std (B10 not-vegetated)
T2_B10_Water = mean (B10 water) + std (B10 water)

The land and water pixels with a B10 value higher than their respective B10 thresholds are classified as cirrus cloud.

If a DEM is present, the elevation information is used to disable cirrus detection above elevations higher than 1500m, in order to avoid false cirrus detection instead of snow detection (see 3.3.3 for details).

Please note that this "cirrus pixels recovery" step is performed only after the post-processing with DEM information.

3.5.7 Bright pixels (Urban and bare soil) recovery with ESA CCI

The scope of this step is use the information contained in the ESA CCI Land Cover maps to improve the cloud detection over urban and bare areas, limiting the false detection of clouds above bright targets like urban buildings or bright soils, without missing true clouds.

3.5.7.1 Use of ESA CCI Land Cover Map

The ESA CCI Land Cover map is used to identify the urban and bare areas (Urban class = 190 and # Bare classes = 200, 201, 202). For these two kinds of land cover, the Fine Morphology algorithm described hereafter is applied to reclassify "unclassified" and "medium probability cloud" pixels into not-vegetated pixels.

3.5.7.2 Fine morphology algorithm

A binary mask is a collection of elements of different size, e.g. depending on the different type of clouds in the scene.

This "fine morphology" algorithm consists in filtering from a binary mask the elements that are spatially close to a type of class(es). This is achieved by computing for each element the percentage of pixels belonging to these classes in its neighbourhood. A "neighbourhood percentage" is then used to discard from the binary mask the elements that satisfy a condition on this neighbourhood percentage (e.g. higher, lower a defined threshold)

- All the elements of the binary mask given as input are labelled with a unique index;
- All elements of the mask are dilated using a 3 x 3 operator;
- The dilation rings over each element are obtained;
- An histogram is computed to obtain the size in pixels of each ring (used latter to compute the neighbourhood percentage);
- The intersection of rings with clouds and cloud shadow mask is computed;
- The neighbourhood percentage for each ring is computed;

- The elements above the neighbourhood percentage are removed from the binary mask

In our case of study, the visual inspection has shown that the binary elements due to false cloud detection of bright buildings are usually isolated from cloud-related classes (medium probability cloud, high probability cloud, cloud shadow and unclassified) and are more likely to be adjacent to cloud-free pixels classes like vegetation or not-vegetated.

On the contrary, binary elements due to true detection of cloud are generally adjacent to other cloud related classes.

Therefore, a cloud-related classes neighbourhood percentage is set to 35% to identify cloud free pixels (e.g. building or bare area). Those pixels are removed from cloud classes and reclassified as not-vegetated pixels.

Please note that this "bright pixels recovery" step is performed only after the post-processing with DEM information.

3.6 Post-processing with DEM information

This step consists in "cleaning" some pixels initially identified as "water", "cloud shadow" or "cloud medium probability", using the information provided by the Digital Elevation Model. Those pixels located in topographic shadows are then reclassified to "dark_features" pixels.

3.6.1.1 With ESA CCI Water Bodies Map:

If the usage of ESA CCI Water Bodies (WBI) map is activated, then only the pixels that are not classified as water pixels in the WBI map, can be reclassified to "dark_features" pixels using the DEM information.

3.6.2 Water pixels cleaning with DEM

The scope of this step is to reclassify as "dark_features" pixels classified as "water" if those pixels are located in mountain shades (topographic shadow) and on steep slopes.

3.6.3 Cloud shadows pixels cleaning with DEM

The scope of this step is to reclassify as "dark_features" pixels classified as "cloud shadows" if those pixels are located in mountain shades (topographic shadow).

3.6.4 Topographic shadows with DEM

The scope of this step is to classify as "dark_features" pixels not classified or initially classified as "medium probability cloud" if those pixels are located in mountain shade (topographic shadow). Most of the pixels addressed by this step are usually pixels covered by snow but not illuminated directly by the sun.

Starting with Sen2Cor version 2.10, a ray tracing cast shadow algorithm based on *"Vectorial algebra algorithms for calculating terrain parameters from DEMs and* *solar radiation modelling in mountainous terrain", JAVIER G. CORRIPIO, Int. J. Geographical Information Science, 2003, vol.17, no 1, 1-23."* has been developed to improve the detection of topographic shadows with low solar angles. It replaces the Gdaldem hillshade algorithm previously used. The processing is done at 20 m resolution by default.

3.7 S2 MSI Parallax characteristics for cloud screening

Since Sen2Cor version 2.10 a new method is implemented based on a novel Telespazio algorithm using OpenCV library. This method is tested to improve the **cloud shadow algorithm** by evaluating the cloud top height and restricting the area for cloud shadow determination. The algorithm with cloud top height estimation is briefly summarized hereafter:

- Estimation using **Sentinel-2 MSI instrumental parallax** between: Band B08 (resampled at 20 m) and B8A
- The **pixel displacement** is computed for the pixels of the cloud mask (novel Telespazio algorithm using OpenCV library)
- Displacement is converted in **cloud top height estimation** (m) using B08/B8A parallax information and pixel resolution *Remark: height above DEM not altitude*
- Statistics on the **cloud height distribution** are computed and used to identify the regions of potential cloud shadow in the image (using sun angles).
- This information is then "crossed check" with potential cloud shadow pixel based on pixel radiometry (as in Sen2Cor v2.8)
- *Clouds with cloud top height below 250 m are discarded from cloud mask for cloud shadow computation*

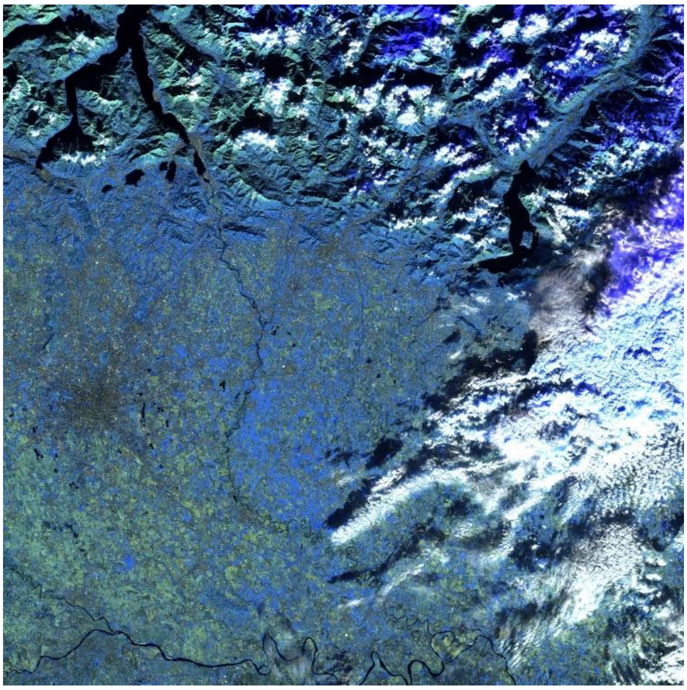

Figure 3-28: Level-1C (RGB with B12, B11, B8A)

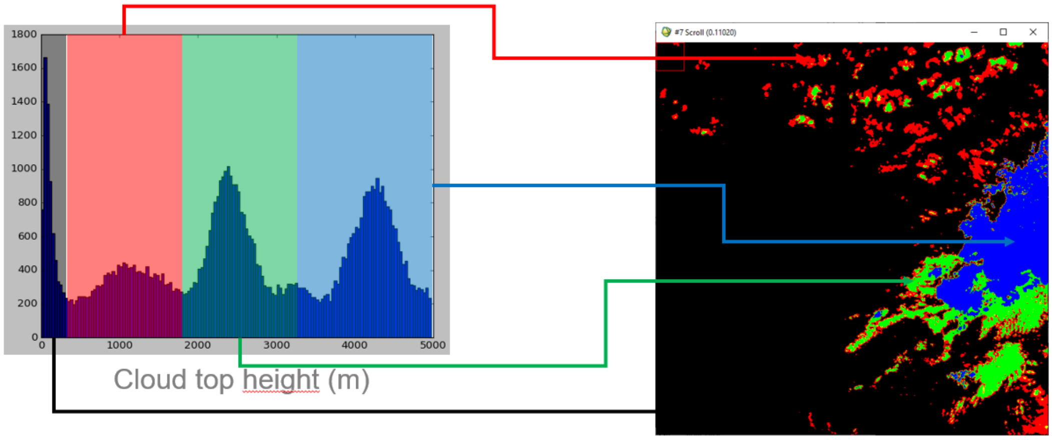

Figure 3-29: Correspondence between cloud top height histogram and different cloud clusters types on the right image

Figure 3-28**Erreur ! Source du renvoi introuvable.** shows a RGB colour composite using SWIR bands (R=B12,G=B11) and NIR band (B=B8A). In this type of colour composites the snow appears usually in blue or purple as snow exhibits lower reflectance in SWIR region than in NIR region. One can see on Figure 3-29 that the histograms could be split in 4 sections (black, red, green, blue). In the image space it corresponds to different types of pixels that could roughly be classified as black: ground, red: low-altitude cloud, medium-altitude cloud, high altitude cloud.

This algorithm is also used to:

1) remove some of bright surfaces/buildings detected as false clouds from final cloud mask. -> identified by very low pixel displacement
2) Pixel displacement could be computed on snow to check that snow pixels are located on ground and not in altitude (false snow in sky) -> identified by medium/high displacement

3.8 Generation of scene classification mask

The scene classification mask (SCL) is generated and updated at each step of the Cloud/Snow detection algorithm described in section 3.2. The cloud classes "cloud_medium_probability" and "cloud_high_probability" are assigned according to the cloud probability derived in the cloud probability mask. It is then further updated at each subsequent step (i.e. cirrus cloud detection, cloud shadow detection, pixel recovery and post-processing with DEM information).

The scene classification map is produced for each Sentinel-2 Level 1C product at 20 m or 60 m resolution. The corresponding byte values of the classification map and the recommended colour table for visualisation are expressed in the Table 3-I hereafter:

Table 3-I – Scene Classification Map (SCL)

Label	Classification
0	NO_DATA

Label	Classification
1	SATURATED_OR_DEFECTIVE
2	CAST_SHADOWS
3	CLOUD_SHADOWS
4	VEGETATION
5	NOT_VEGETATED
6	WATER
7	UNCLASSIFIED
8	CLOUD_MEDIUM_PROBABILITY
9	CLOUD_HIGH_PROBABILITY
10	THIN_CIRRUS
11	SNOW

Please note that this map does not constitute a land cover classification map in a strict sense, its main purpose is to be used internally in Sen2Cor in the atmospheric correction module to distinguish between cloudy pixels, clear pixels and water pixels.

3.9 Cloud and shadow dilation

Since Sen2Cor 2.10 a dilation of clouds and shadows is performed with the following characteristics:

- + 80 m cloud mask
- + 40 m cloud shadow mask
- + 20 m snow mask

The dilation is performed carefully to avoid the dilation of false cloud leading to higher commission error:

- No cloud dilation in shoreline regions (bright sand / white caps issues)
- Only large clouds (>1000 pixels @ 20 m) are dilated above urban areas
- No cloud dilation in soil/snow boundary regions (mixed pixel spectral issue)
- Only cloud with cloud probability > 65% are dilated
- Very small clouds (<= 3 pixels) are not dilated

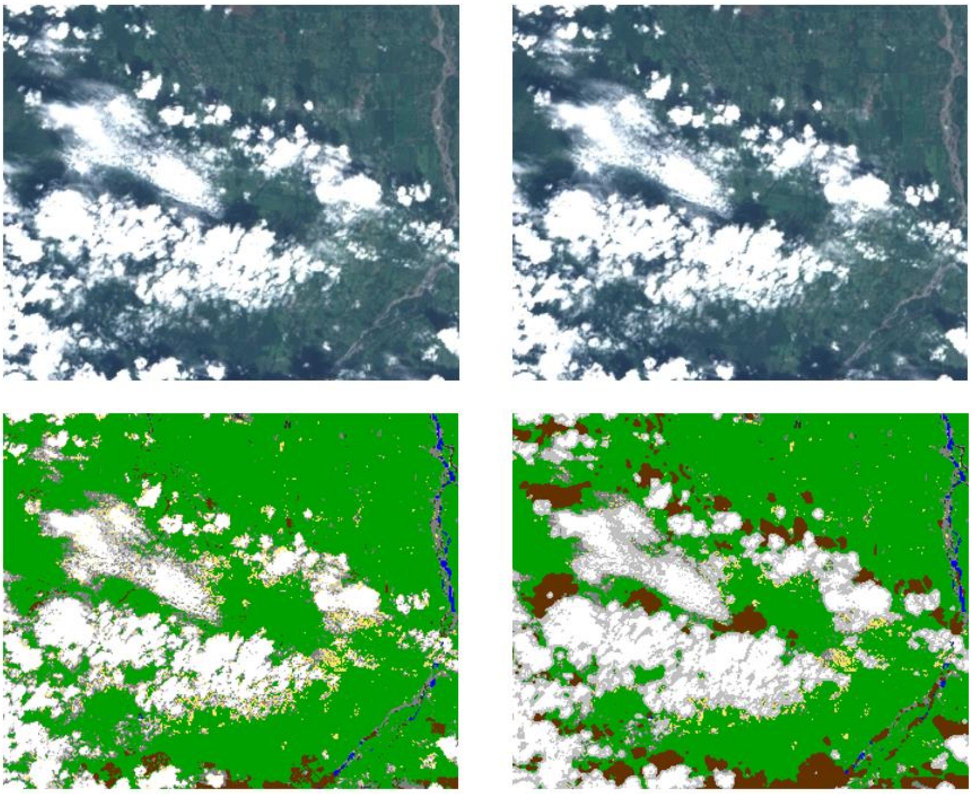

Figure 3-30: Example of SCL dilation
Left: Sen2Cor version 2.8 Right: Sen2Cor version 2.10

4. Atmospheric Correction

This part of the algorithm has to be performed in order to convert multispectral Top of Atmosphere Level 1C image data as inputs to Bottom of Atmosphere L2A image data as outputs. The scope of this conversion is to remove the influence of the atmosphere from satellite observations of the earth surface. This atmospheric correction of satellite images has to deal with two main physical processes – absorption and scattering by gas molecules and aerosol particles in the atmosphere. Scattering by air molecules and absorption by some gases like O_2 and CO_2 are easy to account for. The amount of these constituents in the atmosphere is known sufficient accurate and can be considered as constant over time and space. Amounts of aerosols and other gases like water vapour and ozone are very variable in time and space and have to be estimated for the time and location of satellite data acquisition. The best way is to estimate the amounts of these atmospheric constituents from the satellite data itself. Unfortunately, this atmospheric part of radiation measured by satellites is coupled with the part of radiation reflected by the earth surface.

The joint retrieval of atmospheric constituents and surface reflectance is based on a modelling of the radiative transfer in the earth's atmosphere. In most cases, no information on the bidirectional reflectance behaviour of surfaces is available, and a simple isotropic (Lambert) reflectance law has to be assumed. The libRadtran code [1, 2, 11] was used to compute the relevant atmospheric terms. In spectral regions dominated by scattering effects, calculations are performed with the scaled DISORT option (discrete ordinate radiative transfer [12]). In regions with strong atmospheric absorption the more accurate correlated k algorithm is employed. The results are stored in look-up tables (LUTs).

In a strict sense, the surface reflectance should be called hemispherical-directional reflectance factor (HDRF), or hemispherical-conical reflectance factor HCRF, because the reflected radiation is always measured in a small cone. The anisotropic reflectance behaviour is characterized by the bidirectional reflectance distribution function (BRDF) [13-15]. However, for simplicity we will use the abbreviation surface reflectance instead of HDRF or HCRF.

Figure 4-1 presents an overview on the processing steps included in the atmospheric correction. Before the atmospheric correction takes place a coarse pre-classification of the scene (land, water, cloud, etc), which is part of the already described algorithm in chapter 3. Cirrus correction is an optional pre-processing step. Then the aerosol optical thickness (AOT) and water vapour maps are derived, followed by the surface reflectance retrieval. The details are presented in the next sub-chapters.

Sen2Cor employs the Lambert's reflectance law and assumes a constant viewing angle per sub-scene of 30x30 km^2. The solar zenith and azimuth angles are bilinear interpolated across the scene based on values provided in the metadata for the tile corners.

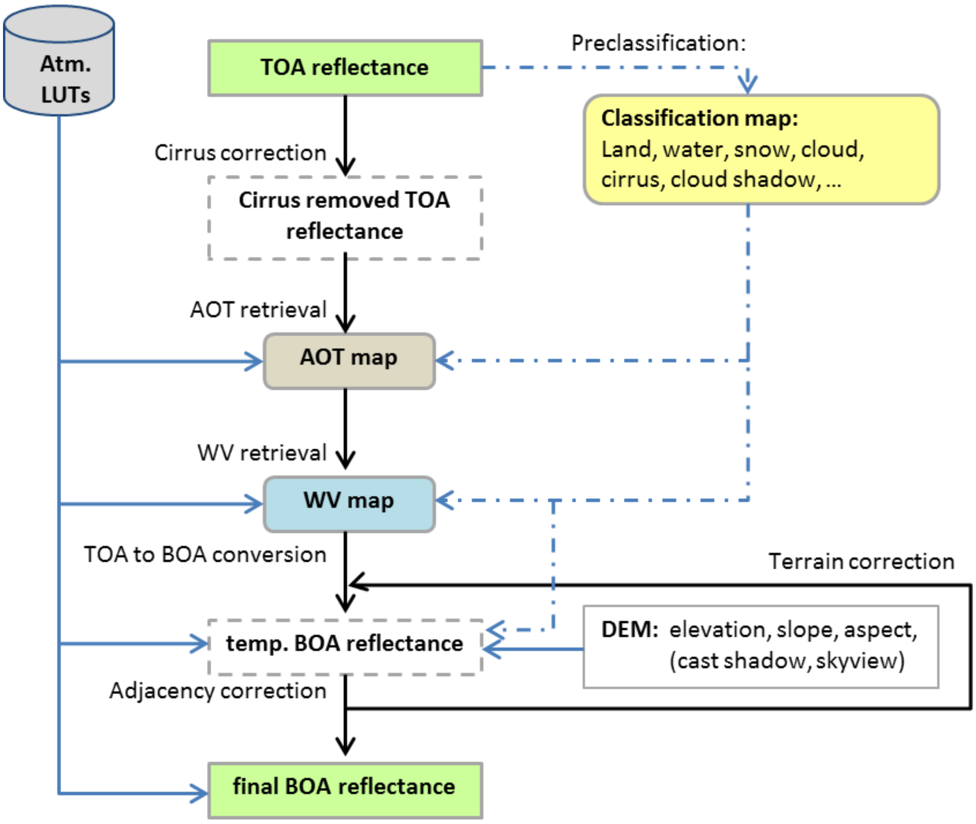

Figure 4-1 – Flow chart of processing

4.1 Database of radiative transfer calculations (LUTs)

Sen2cor is based on the radiation transfer for a large homogeneous Lambertian surface as described by [16, 17]. The relation between the total at-sensor or TOA radiance L and ground reflectance ρ is

$$L(\rho) = L_p + \tau \cdot \frac{E_g(0)}{(1-s\cdot\rho)} \cdot \frac{\rho}{\pi} = L_p + \tau \cdot E_g(\rho) \cdot \frac{\rho}{\pi} \qquad (0.1)$$

where L_p, τ, $E_g(0)$, and s are path radiance, total ground-to-sensor transmittance, global flux on the ground for $\rho = 0$, and the spherical albedo of the atmosphere, respectively. The total transmittance τ is the sum of the direct and diffuse transmittances, i.e., $\tau = \tau_{dir} + \tau_{dif}$. The global solar flux on the ground consists of a direct and a diffuse hemispherical component, i.e., $E_g = E_{dir} + E_{dif}$. The wavelength or spectral band index has been omitted for clarity.

The LibRadtran version 2.0.2 code was employed to calculate a database of all radiative transfer functions in equation (0.1) for different sensor and solar geometries, ground elevations, and atmospheric parameters[6]. These Look-Up-Tables (LUTs) were computed for Sentinel-2A and Sentinel-2B instrument spectral responses [4].

[6] See comment in footnote 1, section 1.1 concerning this approach.

Two radiation transport runs are necessary to provide all radiation components contained in the LUT. The first run with surface reflectance ρ_0=0 provides path radiance L_p and global flux on the ground $E_g(0)$. A second run with ρ_1=0.15 allows to calculate the diffuse ground-to-sensor transmittance

$$\tau_{dif} = \frac{\pi \cdot [L_{path}(\rho_1) - L_{path}(0)]}{\rho_1 \cdot E_g(\rho_1)} \quad (0.2)$$

and over

$$E_g(\rho_1) = \frac{E_g(0)}{1 - \rho_1 \cdot s} \quad (0.3)$$

the spherical albedo

$$s = \frac{\left[1 - \frac{E_g 0}{E_g(\rho_1)}\right]}{\rho_1} \quad (0.4)$$

The following list presents the 6-dimensional parameter space and the grid spacing which is required for each parameter. The atmospheric correction processor reads the LUTs pertaining to this parameter space and interpolates if required. Interpolation is not supported for the aerosol type.

Users are advised that products with a Sun-Zenith Angle (SZA) higher than 70° are processed in Sen2Cor with a clipped SZA value of 70°. This results in an under-correction of the atmospheric signal, which results in a bluish colour on the L2A products. The surface reflectance of products with SZA > 70° should not be used for quantitative/scientific analysis.

Table 4-I: Parameter space for atmospheric correction.

parameter	range	increment / grid points
solar zenith angle	0 -70◦	10◦
sensor view angle	0 -10◦	10◦
relative azimuth angle	0 -180◦	30◦(180◦= backscatter)
ground elevation	0 -2.5 km	0.5 km
visibility	5 -120 km	5, 7, 10, 15, 23, 40, 80, 120 km
aerosol type		rural, maritime
ozone(1)	250-450 DU	250, 290, 331, 370, 410, 450 DU
ozone(2)	250-460 DU	250, 290, 330, 377, 420, 460 DU
water vapour(1)	0.4 -5.5 cm	0.4, 1.0, 2.0, 2.9, 4.0, 5.0 cm
water vapour(2)	0.2 -1.5 cm	0.2, 0.4, 0.8, 1.1 cm

(1): *mid-latitude summer profile,*

(2): *mid-latitude winter profile*

The LUT elevation range is 0 – 2.5 km above sea level. Higher elevations up to 3.5 km are calculated with linear extrapolation of the radiative transfer terms with negligible errors for elevations up to 4 km[7]. The 4 km threshold obviously affects mountainous regions higher than 4 km above sea level. The error impact of processing these regions with the extrapolated height of 3.5 km generally can be considered as small because the highest aerosol concentrations are below 3 km. For the visible bands of S2 the Rayleigh path radiance will be overestimated causing an underestimation of the surface reflectance, which might play an effect for dark surfaces. However, as the regions higher than 4 km are mostly snow covered areas the underestimation effect will be small.

Visibility is used in Sen2Cor as a parameter for aerosol optical thickness (AOT) like in ATCOR. Sen2Cor was developed on basis of ATCOR which is using atmospheric LUTs calculated based on MODTRAN's visibility parameter. Note, that the visibility parameter in Sen2cor and ATCOR is a parameter applied for aerosol content of the vertical atmospheric column. It is different from horizontal visibility at the earth surface. The conversion between visibility VIS and AOT550 (AOT at 550 nm) can be calculated with equation

$$AOT550(z, VIS) = exp(a(z) + b(z) \cdot \ln(VIS)) \quad (0.5)$$

where a(z) and b(z) are obtained with a linear regression for a set of elevations z. The regression is performed with height data between 0 and 2.5 km above sea level. But once the coefficients are calculated, this equation can be applied for $z > 2.5$ km. However, as stated above, the maximum elevation for Sen2Cor is 3.5 km, and elevations greater than 3.5 km are treated as having the maximum elevation.

Over the spectral range of Sentinel-2 (0.44 – 2.2 µm) several molecular absorbers in the atmosphere have to be taken into account (Figure 2-3). Most of them can be assumed with a constant mixing ratio on the global scale, such as oxygen, methane, and CO_2. For CO_2 a constant mixing ratio of 400 ppmv is assumed.

Ozone is known to vary on the global scale. Extreme values of 200 – 500 Dobson Units (DU) can occur, however, a more typical range of values is from 250 - 400 DU. The influence of ozone content on surface reflection retrieval was estimated based on default ozone column of 330 DU at sea level for the mid-latitude summer atmosphere. Figure 4-2 shows the relative error in surface reflectance retrieval for ozone columns of 250 DU and 410 DU when the retrieval is performed with the assumption of a 330 DU column. The four curves correspond to the two ozone columns (250, 410 DU) and two surface reflectance values of $\rho = 0.05$ (dark surface) and $\rho=0.15$ (medium surface reflectance). Retrieval errors of up to 6% can be found in the 400 - 700 nm part of the spectrum. The error is largest in the 550 – 620 nm region for low reflectance surfaces (relative reflectance error about 5 – 6%) decreasing with surface brightness. The maximum relative reflectance error is about 3% for medium reflectance surfaces with $\rho = 0.15$. The calculation was performed with MODTRAN4 using the parameters: mid-latitude summer atmosphere, rural aerosol, visibility 23 km, water vapour column 2.9 cm, solar zenith angle 40°, ground at sea level.

Ozone information cannot be retrieved from Sentinel-2 data. Vertical column ozone content is available within the auxiliary data of the Sentinel-2 L1C granule as a 9 by 9 pixels grid with a pixel resolution of 0.125 degree in geographic projection. The source of this ozone dataset is ECMWF (http://www.ecmwf.int/).

[7] Ground elevation can theoretically be extended up to 8 km. However, this would increase the size of S2 database that has to be calculated.

LUTs are provided for a discrete set of ozone columns (sea level to space) both for a midlatitude summer and winter atmospheric model. The ozone information provided in the L1C auxiliary data can be used in Sen2Cor to automatically select the set of LUTs generated with the ozone column with the nearest value (e.g. one of 250, 290, 331, 370, 410, 450 DU). No interpolation is performed between LUTs with different ozone columns, i.e if ECMWF ozone gives a value of 360 DU, the set of LUTs generated with ozone equal to 370 DU is selected, not an interpolation between the LUTs of 331 DU and 370 DU.

Recommended baseline processing are the LUTs for summer atmospheric profile. The use of winter LUTs is recommended based on geography and climatology, because the use of summer LUTs under winter conditions yields relative surface reflectance retrieval errors up to 8% for bands beyond 700 nm.

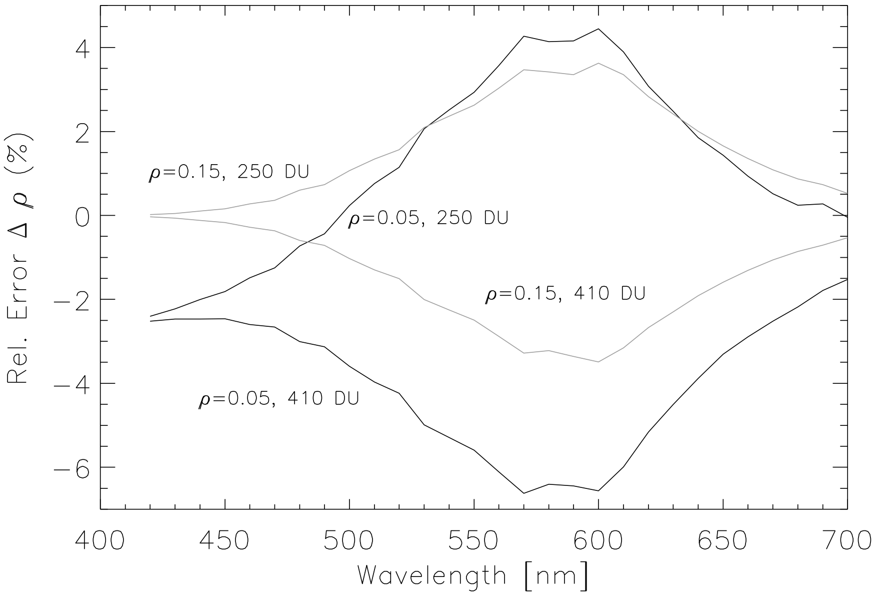

Figure 4-2 – Relative surface reflectance errors due to ozone

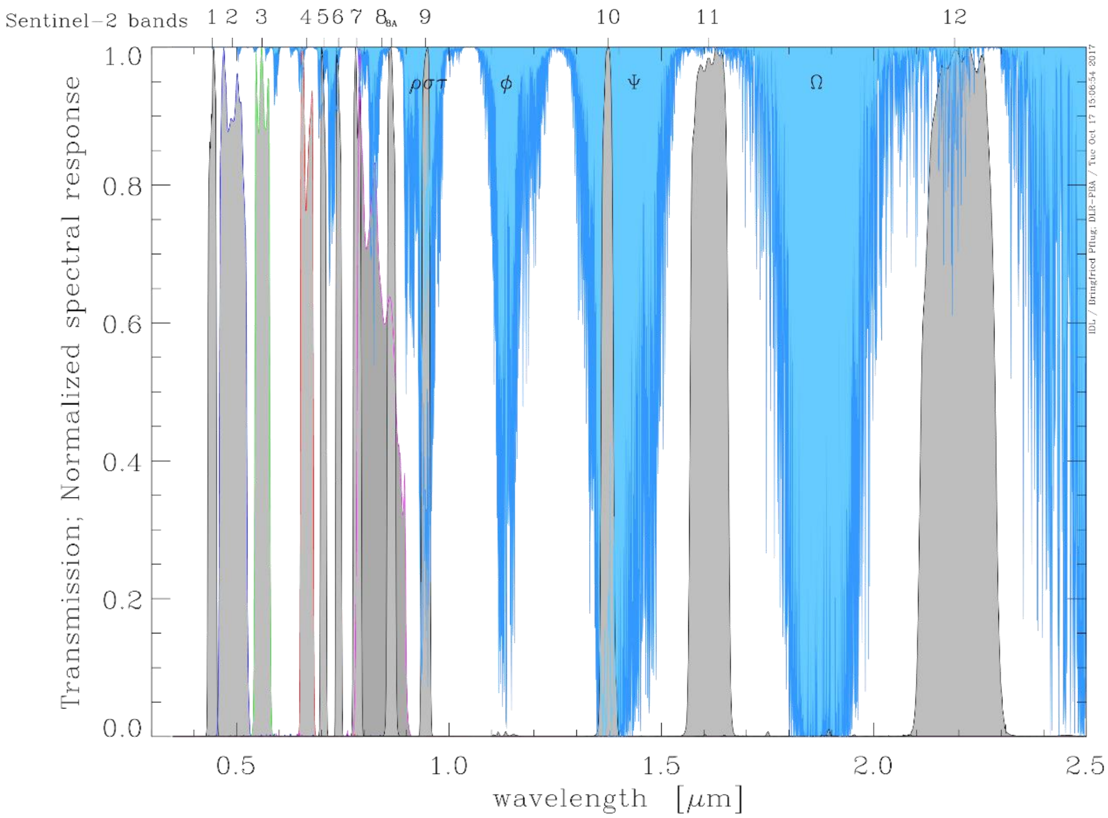

Figure 4-3 – S2A spectral response functions and transmission due to vertical column WV absorption for subarctic winter atmosphere (light blue, lowest WV content) and tropical atmosphere (darker blue, highest WV content). WV transmission data originate from MODTRAN [5].

The influence of water vapour absorption on the different Sentinel-2 bands is demonstrated in Figure 4-3 by providing optical transmission for the driest and the most wet model atmospheres.

WV is retrieved by Sen2Cor on a per-pixel basis with the band 8a (865 nm) and band 9 (945 nm). LUTs are provided as for ozone for a discrete set of WV columns (sea level to space) both for midlatitude summer and winter atmospheric models. Opposite to ozone, LUT interpolation will be performed for WV during surface reflection retrieval.

Look-up-table selection can be influenced by the user editing the L2A_GIPP.xml file located in the Sen2Cor home directory of the user. More detailed information about processing configuration can be found in Sen2Cor Configuration and User Manual [S2-L2A-SUM].

4.2 Cirrus removal pre-processing

On the first glance, images contaminated by cirrus appear similar to hazy scenes. However, haze usually occurs in the lower troposphere (0-3 km) while cirrus clouds exist in the upper troposphere and lower stratosphere (8 -16 km). The effect of boundary layer haze can be observed in the visible region, but seldom in longer wavelength bands > 850 nm. Cirrus affects both the NIR and SWIR spectral regions. Thin cirrus clouds are difficult to detect with broad-band multispectral satellite sensors in the atmospheric window regions, especially over land, because land scenes are spatially inhomogeneous and this type of cloud is partially transparent. On the other hand, water vapour dominates in the lower troposphere and usually 90% or more of the atmospheric water vapour column is located in the 0-5 km altitude layer. Therefore, if a narrow spectral band is selected in a spectral region of very strong water vapour absorption, e.g., around 1.38 μm as Sentinel-2 band 10, the ground reflected signal will be totally absorbed, but the scattered cirrus signal will be received at a satellite sensor. So the narrow band 10 at 1.38 μm is not only able to detect cirrus clouds. It can also be used to remove the cirrus contribution from the radiance signal to obtain a cirrus-corrected scene[8].

Cirrus removal is conducted as an optional preprocessing step during atmospheric correction, followed by the aerosol and final water vapour retrievals. It includes preliminary water vapour column estimation to switch off cirrus removal if the average water vapour column W of a scene is less than some threshold (default W=0.25 cm). This shall avoid misinterpretation of bright surfaces as cirrus in the 1.38 μm band. Normally, atmospheric water vapour completely absorbs surface features in the 1.38 μm band, but the band might become partly transparent to surface features for very low water vapour values or higher elevated surfaces.

The basic ideas of cirrus correction were presented in several papers [18-20] in terms of the apparent (TOA or at-sensor) reflectance ρ^{TOA}. It is defined as:

$$\rho^{TOA} = \frac{\pi \cdot L}{E_S \cos\theta_S} \tag{0.6}$$

where L is the recorded radiance signal, E_s the extra-terrestrial solar irradiance for the selected band, and θ_s is the solar zenith angle. Following [18] the implemented method can be described by the following set of equations:

$$\rho^{TOA}(\lambda) = \rho_c^{TOA}(\lambda) + \frac{T_c(\lambda) \cdot \rho(\lambda)}{1 - s_c(\lambda) \cdot \rho(\lambda)} \tag{0.7}$$

Here, ρ_c^{TOA} is the reflectance of the cirrus cloud, T_c the two-way transmittance (direct plus diffuse) through the cloud, ρ the reflectance of the *"virtual"* surface below the cirrus (including all effects of molecular and aerosol scattering below the cirrus and reflection of land or water surface), and s_c is the cloud base reflectance of upward radiation. As the cirrus is almost on top of the atmosphere we use ρ^{TOA}_c (λ) instead of the reflectance of the cirrus cloud $\rho_c(\lambda)$ at its altitude. Equation (0.7) can be simplified, because of $s_c\,\rho \ll 1$, yielding

$$\rho^{TOA}(\lambda) = \rho_c^{TOA}(\lambda) + T_c(\lambda) \cdot \rho(\lambda) \tag{0.8}$$

With the assumption that the cirrus reflectance $\rho_c^{TOA}(\lambda)$ for any band is linearly related to the cirrus reflectance at 1.38 μm we obtain

$$\rho_c^{TOA}(\lambda) = \rho_c^{TOA}(1.38\mu m)/\gamma \tag{0.9}$$

[8] The parallax difference between the cirrus band and other bands is up to 0.81°. The parallax error will be compensated in the ortho-rectified product at the ground surface. However, a parallax error will remain at the cirrus altitude level. As cirrus altitudes cannot be calculated from Sentinel-2 imagery and may vary between typically 8 and 20 km the corresponding spatial misregistration is up to about 300 m. So the issue of cirrus removal is left open.

where γ is an empirical parameter. It depends on the scene content, cirrus cloud height, and solar and viewing angles. The derivation of this empirical parameter differs for water and land pixels. For water, a scatterplot of the 1.38 μm band versus B8a (865 nm) is used and for land the band-correlation is determined from a scatterplot of the 1.38 μm band versus the red band B4 (665 nm). To obtain a high sensitivity over land, only vegetation pixels are taken preferably. They have a low reflectance in the red spectral region, so that the cirrus contribution is easily traced. Figure 4-4 shows an example of such a scatterplot. The red line is the left-side boundary of data points that are not influenced by ground surface reflection, i.e. cirrus-contaminated pixels are clustered around this line, and its slope represents the correlation coefficient γ (the blue line represents the first of several iterations).

Papers on the cirrus algorithm often restrict eq. (0.9) to the wavelength interval 0.4 $<\lambda<$ 1 μm, but [21] extended this relationship into the SWIR region. Substituting equation (0.9) into equation (0.8) yields

$$T_c(\lambda) \cdot \rho(\lambda) = \rho^{TOA}(\lambda) - \rho_c^{TOA}(1.38\mu m)/\gamma \tag{0.10}$$

Neglecting the cirrus transmittance T_c (i.e., setting T_c = 1), we obtain

$$\rho_{cc}(\lambda) = \rho^{TOA}(\lambda) - \rho_c^{TOA}(1.38\mu m)/\gamma \tag{0.11}$$

which is passed as the *"cirrus path radiance corrected"* apparent reflectance image (index 'cc') at top of atmosphere to the subsequent processing.

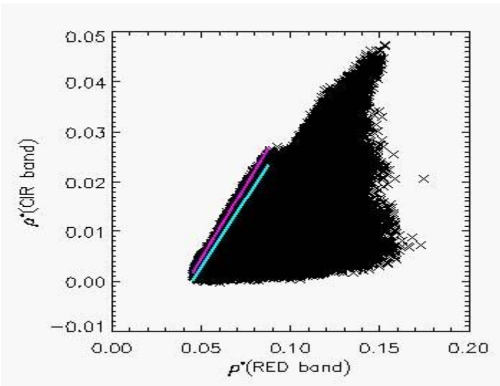

Figure 4-4 – Scatterplot of apparent reflectance of cirrus (1.38 µm) band versus B4 (red band)

4.3 Retrieval of aerosol optical thickness

The problem of AOT retrieval consists in the coupled radiation transport between atmosphere and surface. The TOA signal measured by satellites depends both on surface reflection and aerosols. Consequently, AOT can be estimated only if surface reflection is known.

Copernicus Sentinel-2 MSI has the appropriate spectral bands to derive the aerosol optical thickness of the atmosphere and the aerosol type, provided the scene contains reference areas of known spectral reflectance behaviour [22]. Preferred reference areas are dense dark vegetation (DDV) pixels, because an empirical correlation was found between SR of DDV pixels in the SWIR and in the red region of the spectrum.

The first step of AOT retrieval based on DDV-pixels is estimation of SR in the SWIR. Then an empirical correlation for DDV-pixels between SR in the SWIR and the red band (B4) is applied giving the SR in the red band (B4). Known SR in the red band allows computation of AOT in this region of the spectrum over the DDV-area.

The present approach has similarities and some differences to Kaufman [22, 23] and Liang [24]. All these algorithms rely on DDV and water bodies. Different is that Sen2Cor supports a variable aerosol model. Another advantage of Sen2Cor is that the algorithm includes an iteration to reduce negative reflectance values. Sen2Cor also provides a fall-back solution in case that the scene doesn't contain reference areas. Available fall-back solutions are to use a default value or, if available, to get aerosol content from CAMS data [25].

This section starts with an explanation of the algorithm used to find DDV (reference) pixels, followed by explaining the AOT retrieval and aerosol type estimation based on DDV-pixels. Then information is given about the available fall-back solutions for AOT retrieval and refinement of AOT to avoid negative reflectance values.

4.3.1 Detection of reference (DDV) pixels

Masking reference (DDV) pixels is independent from the scene classification implemented in Sen2Cor which relies on TOA data. The granule is searched for dark (or medium brightness) pixels in the SWIR2 band (B12 at 2.19 μm) relying on SWIR2 BOA-reflectance computed using the start visibility set in the configuration file. Default value of the start visibility is 40 km which corresponds to AOT550 of about 0.20 at sea level. Water pixels are excluded from masking as reference pixels by employing only those pixels with SWIR reflectance values above 1% and an NDVI > 0.1. The upper reflectance threshold for dark reference pixels is first set to 5% in the 2.2 μm band. If the number of reference pixels found with this threshold is less than 2% of the image data pixels, then the upper reflectance threshold is increased to 10% or finally to 12%. A validation and accuracy assessment of the method can be found in [22, 24]. If the SWIR2 band would fail, the 1.6 μm band could be taken as a substitute. In that case the corresponding upper reflectance thresholds are 10%, 15%, or finally 18%, respectively.

The upper reflectance threshold finally applied for detecting DDV pixels can be found in the processing report file. It gives a good quality indicator for AOT retrieval. The statistical difference of estimated AOT to reference values from AERONET is decreased from 0.133 ± 0.085 to 0.075 ± 0.057 if the validation analysis is limited to granules with DDV-pixels determined with the upper threshold 5% for the dark reference pixels. On the other side the number of detected DDV pixels is remarkably reduced. The number of granules found to have more than 1% reference pixels is decreased by about two third applying this lower reflectance threshold.

4.3.2 AOT retrieval based on DDV pixels

Once the DDV-pixels are detected, SR in the SWIR2 band (B12) is computed presuming a typical value for AOT(SWIR2). SR dominates TOA reflectance in the SWIR so that variations of AOT(SWIR2) over time can be neglected and using a pre-defined, typical AOT value gives a good estimation of SR in B12. The value of

AOT(SWIR2) used at this point can be influenced by the user with setting the Visibility in the configuration file.

Then empirical correlations are employed to compute the SR for B4 (red) and B2 (blue) from obtained SR in B12:

$$\rho_{0.665}^{DDV} = 0.5 \cdot \rho_{2.2}^{DDV} \qquad and \qquad \rho_{0.490}^{DDV} = 0.5 \cdot \rho_{0.665}^{DDV} + 0.005 \quad (0.12)$$

A typical DDV-spectrum showing these relations is sketched in Figure 4-5 (left).The offset 0.005 for the blue band yields a better correlation with ground based measurements than zero offset [26]. If the SWIR2 band would fail, the 1.6 μm band could be taken as a substitute replacing the first empirical correlation by.

$$\rho_{0.665}^{DDV} = 0.25 \cdot \rho_{1.6}^{DDV} \quad (0.13)$$

The correlation factor of 0.5 between the 2.2 μm and the red region is not a universal constant, but may typically vary between 0.4 and 0.6. The correlation actual also works for dark soils. So the dark (reference) pixels may also include soil areas. As the correlation factor may in general depend on the biome, season, and geography, an update of the DDV model would improve the accuracy of the aerosol retrieval. A seasonal DDV model was proposed for large boxes (about 10 km × 10 km) of MERIS data [27], but world-wide DDV model maps at a spatial resolution of about 100 m are currently not available.

Now SR for B4 (red band) is known and used for estimation of AOT550. However, the original calculation is performed in the visibility space, because the atmospheric LUTs were calculated based on MODATRAN visibility parameter. Refer to section 4.1 for conversion between AOT and visibility (VIS). LUTs are precomputed for visibility range 5-120 km which corresponds to AOT range from 1.12 to 0.08 at sea level.

Visibility is found as the intersection of the measured radiance with the computed visibility-dependent at-sensor radiance curve provided by the LUT for the obtained SR of B4 and geometry (compare Figure 4-5 right).

Sen2Cor employs internally in place of continuous VIS an integer visibility index ('vi') ranging from vi=0 to vi=182 for a fast indexing of arrays depending on visibility. This avoids time-consuming interpolation. Visibility index is closely related to total optical thickness at 550nm

$$Total\_OT_{550} = 0.185 + 0.006\, vi \quad (0.14)$$

AOT550 can be easily computed from total optical thickness at 550 nm subtracting optical thickness for Rayleigh scattering (0.10 at sea level) and ozone absorption (0.03). Visibility index vi=0 corresponds to VIS=173 km at sea level.

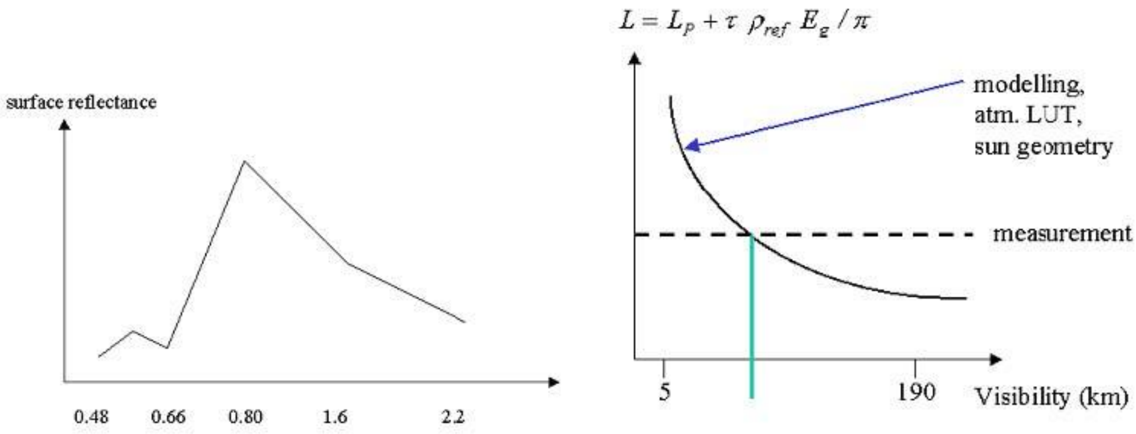

Figure 4-5 – Correlation of reflectance of dark vegetation in different spectral regions and visibility calculation

Once the visibility has been calculated for the dark reference pixels, the average VIS for the DDV-pixels is taken for the non-reference pixels, and the corresponding map is smoothed with a 1 km x 1 km Gaussian spatial filter to remove noise and to suppress small-scale fluctuations that might be caused by biome-dependent changes in the spectral correlation. Experience with MODIS has shown that a large spatial filter size is necessary to avoid artefacts [28].

Whereas the complete subsequent processing makes use of visibility-index map, this map is finally converted to AOT for exporting. AOT-map is smoothed again with a Gaussian filter to smooth the discrete values of visibility-index map.

4.3.3 Aerosol type estimation based on DDV pixels

Aerosol type is constant per scene in the Sen2Cor model. Aerosol type can be set fixed to rural/continental or maritime model or the optional aerosol type estimation can be used. The scene path radiance in the blue (B2) and red (B4) region is computed for optional aerosol type estimation as total measured minus reflected radiance, using the average values for the dark reference pixels.

$$L_p^{granule}(\rho_{DDV}) = L_{DDV}^{Sentinel2} - \tau \cdot E_g(\rho_{DDV}) \cdot \frac{\rho_{DDV}}{\pi} \qquad (0.15)$$

The average ratio of $L_p^{granule}(blue)$ to $L_p^{granule}(red)$ is then compared to the corresponding ratio computed with the implemented LibRadtran standard aerosols (rural, maritime) from the look up tables:

$$dp = \frac{\frac{L_p^{granule}(blue)}{L_p^{granule}(red)}}{\frac{L_p^{LUT}(blue)}{L_p^{LUT}(red)}} \qquad (0.16)$$

The aerosol type for which the double ratio (d_p) is closest to 1 is the best approximation for the scene.

The question arises whether the automatic selection is the best choice, especially if one considers neighbouring scenes. In this case the aerosol types could switch, leading to steps in the surface reflectance at the image borders. From this point of view a pre-selected aerosol type (e.g. rural-continental) might be the better choice in practice.

4.3.4 Blue path radiance rescaling on DDV pixels

Some fine tuning called 'blue path radiance rescaling' (BPRR) can be subsequently performed with the selected aerosol type fixed. BPRR enables to adjust the limited set of standard aerosol types available in the LUT to the actual spectral behaviour of the path radiance in the blue spectral region. The blue path radiance $L_p^{granule}(blue)$ is computed again with equation (0.15)(0.15)(0.15) as total measured radiance in the blue minus reflected radiance computed for SR, VIS and selected aerosol type estimated for DDV pixels. If $L_p^{granule}(blue)$ deviates more than 5% from $L_p(blue, LUT)$, then $L_p^{granule}(blue)$ is used as the valid path radiance. In addition, the path radiance for any other bands in the blue to red region is linearly re-scaled with the factor $L_p^{granule}(blue, scene)$ /$L_p^{granule}(blue, LUT)$, see Figure 4-6. The path radiance in B4 is used as a fixed tie point. Path radiance is not corrected for wavelengths greater than 700 nm, because path radiance contributes only a small fraction to the total radiance in the NIR and SWIR and because the difference in path radiance between the selected aerosol type and the actual aerosol is typical less than 10% in this region of the spectrum.

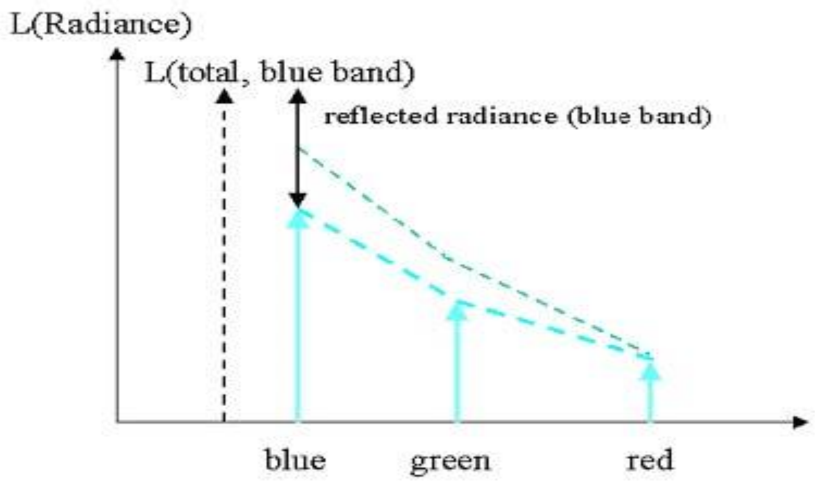

Figure 4-6 – Rescaling of the path radiance with the blue and B4

Blue path radiance rescaling is switched off in the default configuration of Sen2Cor because it led to overcorrection for some products. It can be switched on and configured by advanced users.

4.3.5 Fall-back algorithm using a default AOT (option 1)

If the scene contains less than 1% reference pixels, then no AOT-estimation is possible with the DDV-algorithm and a fall-back solution is necessary. There are two options for a fall-back solution within Sen2Cor. Option 1 is to generate an AOT map on basis of the start visibility set in the configuration file. This is a good option if you know actual AOT for the granule to process which you can convert to VIS. Note that AOT depends on surface elevation and that exported AOT map can contain AOT variations in case of rugged terrain even for a constant visibility set per granule.

4.3.6 Fall-back algorithm using meteorological AOT CAMS (option 2)

Fall-back solution option 2 is taking the required AOT map from external sources. Total aerosol optical thickness data at 550 nm are provided globally by the Copernicus Atmosphere Monitoring Service (CAMS) managed by ECMWF [29]. This meteorological AOT can be used by Sen2Cor as a fall-back solution for the DDV algorithm.

AOT information needs to be available either in auxiliary data of L1C product or in the Sen2Cor auxiliary data folder.

<u>Overview of meteorological CAMS AOT usage:</u>

Figure 4-7 presents the overview of the CAMS aod algorithm in Sen2Cor. It replaces the previous fallback solution that is based on a user defined constant value, used when the percentage of Dark Dense Vegetated pixels was not enough.

When DDV < 1%, the fallback solution relying on CAMS data [CAMS] is activated to generate a final visibilities map used in Sen2Cor atmospheric correction subsequent processing.

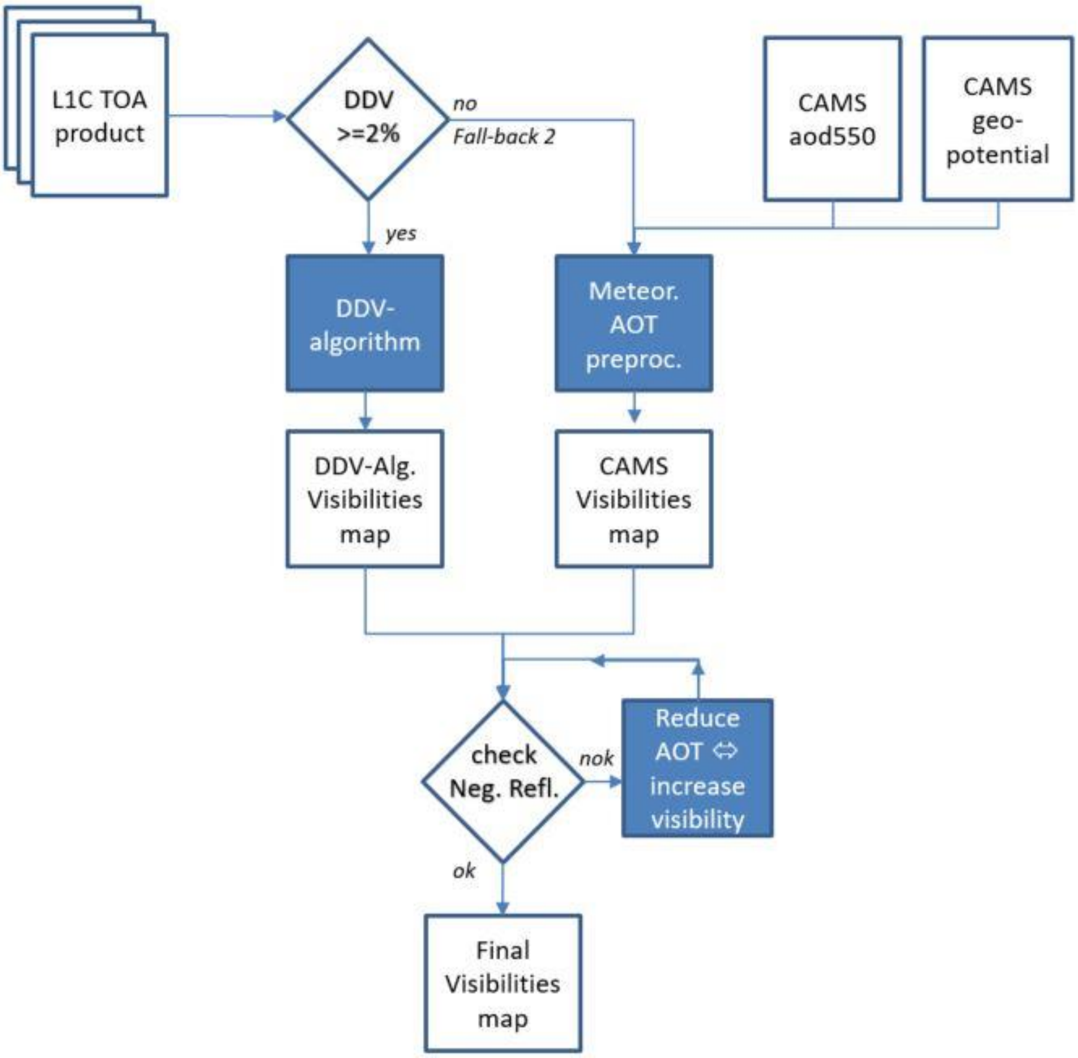

Figure 4-7: Overview of CAMS AOT algorithm in Sen2Cor

Meteorological AOD data pre-processing

The pre-processing step includes a temporal interpolation (linear) to the Sentinel-2 acquisition time as well as spatial extraction and resampling to Sentinel-2 geometry (cubic spline). Implementation details are provided hereafter:

1) The two nearest NETCDF files in term of acquisition date are identified in the ECMWF/CAMS local directory;
2) These two files are converted from AOT to visibility (at the altitude of the geopotential) using a formula provided by DLR/ATCOR;
3) A visibility map is interpolated to the Sentinel-2 acquisition time (linear) using in inputs the two visibility maps generated in previous step;
4) This visibility map is resampled to the Sentinel2 tile grid (cubic spline)
5) A VIM band (for VIsibility Meteorological) is created from this array. Numerical values are coded in km with a factor 100. (2 km ⬄ 200 DN)
6) This extra VIM band is loaded in Sen2Cor (after bands, DEM, and CCI imports)

Usage of VIM band in Sen2Cor (L2A_AtmCorr.py)

In L2A_AtmCorr, if the VIM band exists, it will be used in case of not enough DDV are found:

1) Visibilities are converted in index of visibilities (ATCOR internal format).
2) Mean value of the tile is computed (meanvi CAMS)
3) Meanvi CAMS passes through the check negative function. Only classes 4 and 5 ("vegetation" and "not vegetated") are taken into account for the computation of the percentage of negative pixels.
4) The method gives an updated value of the mean value (meanvi check_neg).
5) All visibilities indexes that are greater that the revised mean value are increased by an offset equal to meanvi(check_neg) - meanvi(CAMS)
6) Visibilities indexes are exported to VIS band. VIS band is the band that is used for the reflectance computation (rho retrieval step 1).

After the VIS band export step the atmospheric correction algorithm continues as in its original version.

4.3.7 Reduction of negative reflectance values

The last step with regard to AOT estimation is an iteration for reduction of negative reflectance values. The visibility index map generated by any of the discussed options is applied for correction of the atmospheric influence from the image (Refer to section 4.6) to get SR images per band. It may occur that the resulting SR-images contain pixels with negative reflectance values due to overestimation of AOT. Water surfaces are most sensitive to AOT overestimation because they typically have very low surface reflectance in the NIR. Therefore, if the scene contains water bodies, the water reflectance in B8a resp. B8 (NIR band) of the resulting BOA product is checked for negative reflectance pixels. If those are encountered, the visibility is increased (corresponds to decreasing AOT) until the percentage of negative reflectance pixels is less than 1% of the scene pixels. The iteration steps are given in Table 4-II. In addition to B8, B4 is also checked for negative reflectance pixels (vegetation). An update of the visibility with respect to the specified input value is noticed in the processing report.

Table 4-II – Visibility iterations on negative reflectance pixels (B2, B8)

visibility [km]	vis. increment [km]
VIS < 23	VIS = 23
23 ≤ VIS < 26	+= 3
26 ≤ VIS < 30	+= 4
30 ≤ VIS < 40	+= 5
40 ≤ VIS < 100	+= 10
100 ≤ VIS	VIS=120 km

4.4 Retrieval of water vapour

Water vapour retrieval is performed after the aerosol retrieval because the aerosol retrieval does not use water vapour sensitive spectral bands, but the water vapour algorithm depends on aerosol properties. The water vapour retrieval over land is performed with the APDA (atmospheric precorrected differential absorption) algorithm [6] which has to be applied to Sentinel-2 bands B8a (865 nm) and B9 (945 nm). Band 8a is the reference band in an atmospheric window region and band B9 is the measurement band in the WV absorption region. The absorption depth is evaluated as sketched in Figure 4-8 (line from point A to B) where the depth of the absorption feature (A –B) is a measure of the water vapour column content.

The water vapour dependent APDA ratio is calculated as:

$$R_{APDA}(u,\rho) = \frac{L_{B9}^{Sentinel-2}(u,\rho_{B9}) - L_{p,B9}^{LUT}(u,\rho_{B9})}{L_{B8a}^{Sentinel-2}(u,\rho_{B8a}) - L_{p,B8a}^{LUT}(u,\rho_{B8a})} \quad (0.17)$$

where L and L_p are the measured total at-sensor radiance and the path radiance computed from the LUT applying (0.15) to all land pixels, respectively. Note that path radiance computation from the LUT depends on ρ. The symbol u indicates the water vapour column content.

The problem is the estimation of the surface reflectance ρ_{B9} in the absorption band. Here the assumption $\rho_{B9} = \rho_{B8a}$ is used for two reasons. First, the surface reflectance at B9 is difficult to assess from the other bands (e.g. due to non-linear reflectance behaviour of vegetation, iron content of soils), and second, the other bands are marginally dependent on water vapour.

LUTs are calculated for different atmospheric water vapour columns and sun angles and an exponential fit function can be used to calculate the relationship between R_{APDA} and u

$$R_{APDA}(u) = exp\left(-\alpha + \beta\sqrt{u}\right) \quad (0.18)$$

which can be solved for the water vapour column u,

$$u = \left(\frac{\alpha = ln(R_{APDA}}{\beta} \right)^2 \quad (0.19)$$

The relationship is plotted in Figure 4-9, where the diamonds in the figure mark the water vapour grid points (u= 0.4, 1.0, 2.0, 2.9 cm) in the LUT.

Equations (0.17) to (0.19) are iterated, starting with u=1.0 cm, calculating RAPDA, updating u, $L_{p,\,I}(u)$, ρ_{B8a} and repeating the cycle.

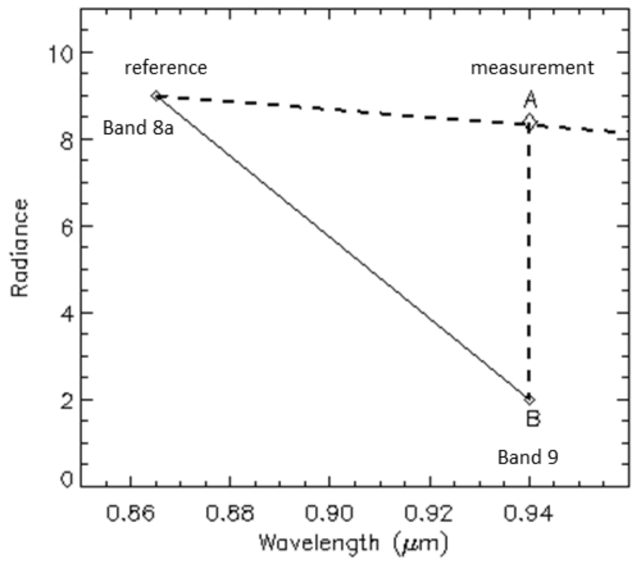

Figure 4-8 – Reference and measurement bands for the water vapour method

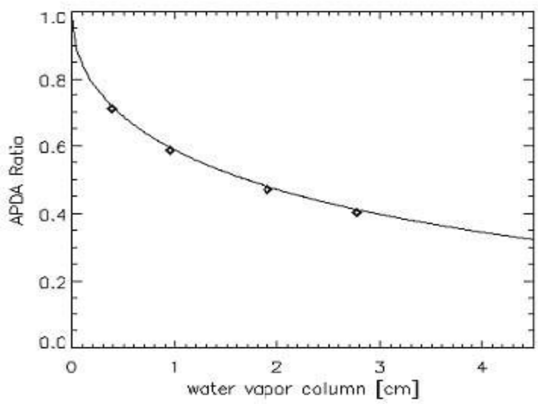

Figure 4-9 – APDA ratio with an exponential fit function for the water vapour

Remarks:

The APDA algorithm is relatively fast. Its disadvantage is that it is not stable numerically for very low reflectance targets (water, shadow regions). For water surfaces the scene-average value of the land water vapour column is taken as a default. Several other options how water pixels are filled with WV-values can be configured by the user.

Five water vapour grid points at 0.4, 1.0, 2.0, 2.9, and 4.0 cm are sufficient to cover the 0.5 to 5.0 cm range with an accuracy of about 5-10 % [30]. The grid point 5.0 cm was recently added for the summer atmosphere to improve the accuracy in the 4.5 – 5.5 cm range.

For winter conditions, a typical winter altitude profile of air temperature / humidity should be selected (the libRadtran mid-latitude winter) to improve the accuracy of the water vapor and surface reflectance retrievals in such conditions. In this case the water vapor grid points are 0.2, 0.4, 0.8, and 1.1 cm.

WV estimation is performed for the default processing baseline. It can be switched off by the user in the configuration file L2A_GIPP.xml located in the Sen2Cor home directory of the user.. Default is use the scene average of water vapour column for water pixels. The user can change the length of square box for smoothing the WV map.

4.5 Correction of Adjacency effect

The total radiation received at a sensor from a pixel consists of three main components:

1. Path radiance giving the part of radiation which is only scattered in the atmosphere without being reflected at the ground.
2. Radiation reflected from the pixel of interest at the ground due to incoming direct and diffuse radiation.
3. Radiation reflected from pixels around the pixel of interest and scattered into the line-of-sight of the sensor.

Only the second radiation component contains the desired information about the reflectance of a pixel. The last component is the so called adjacency radiation which depends on the reflectance of the pixels around. Atmospheric correction has to correct for this part of radiation additionally to correction for path radiance and extinction of the direct light beam. Sen2Cor accounts for adjacency effect during surface reflectance retrieval (see 4.6).

The adjacency effect depends on the aerosol height distribution (among other factors). As this height distribution is not known for operational purposes, a typical horizontal adjacency range of 1 km is assumed, i.e., the standard adjacency kernel window size is 2 km. The adjacency range is not a critical parameter for most pixels, as the influence of the adjacency effect primarily depends on the pixel-to-background reflectance contrast and field patterns tend to repeat itself, i.e. the average reflectance in a 2x2 km^2 adjacency window is usually very close to the value for a 4x4 km^2 window. However, modification of this default adjacency range of 1 km is recommended for dark pixels in a bright neighbourhood like water pixels of a lake in the NIR spectral region surrounded by forest. The adjacency range can be modified by the user in the configuration file L2A_GIPP.xml.

4.6 Reflectance retrieval in flat terrain

As Sentinel-2 L1C data are already converted into TOA reflectance and SEN2COR needs scaled radiance as input, the TOA reflectance has to be converted into TOA radiance

$$L(k) = \frac{E_s(k)\cos\theta_s}{\pi d^2}\rho_{TOA}(k) \qquad (0.20)$$

where k, E_s , θ_s , and d are band index, extraterrestrial solar irradiance for an astronomical distance of 1, solar zenith angle, and sun-earth distance in astronomical units, respectively. E_s depends on the spectral solar irradiance database [31].

In case of image data, the surface reflectance varies from pixel to pixel. Following steps for surface reflectance retrieval are performed for each pixel of the image and for each band:

Step 1: The influence of the neighbourhood (adjacency effect) is neglected and the surface reflectance is obtained from

$$\rho^{(1)}(x,y) = \frac{\pi \cdot (L(x,y) - L_p)}{\tau \cdot E_g} \qquad (0.21)$$

Step 2: The second step calculates the average reflectance in a large neighbourhood of each pixel

$$\bar{\rho} = \frac{1}{N^2}\sum_{i,j=1}^{N}\rho_{i,j}^{(1)} \qquad (0.22)$$

where N corresponds to the number of pixels for the selected range R of the adjacency effect [32]. The exact choice of R is not critical since the adjacency influence is a second-order effect. Instead of the range-independent weighting in equation (0.22), a range-dependent function could be selected with an exponential decrease of the weighting coefficients [32]. However, except for special landscapes the average reflectance over a large adjacency box (2 R x 2 R) usually does not change much as a function of range, because field patterns are repeated. So a range-independent weighting is performed as it reduces the processing time.

Step 3: The reflectance of equation (0.21) is corrected for the adjacency influence

$$\rho^{(2)}(x,y) = \rho^{(1)}(x,y) + q\{\rho^{(1)} - \bar{\rho}(x,y)\} \qquad (0.23)$$

where the function q indicates the strength of the adjacency effect. It is the ratio of the diffuse to direct ground-to-sensor transmittance, i.e.

$$q = \tau_{dif} / \tau_{dir} \qquad (0.24)$$

Surface reflectance retrieval can run for flat terrain only without terrain correction. If a DEM is provided, it is used only for AOT- and WV retrieval and to compute the average altitude of the granule. If no DEM is available, then the ground altitude has to be set in the configuration file.

4.7 Reflectance retrieval in mountainous terrain

In mountainous terrain the topography introduces strong brightness variations depending on the orientation of a surface element. The objective of a combined topographic / atmospheric correction is the elimination of topographic effects during the surface reflectance retrieval. Surfaces oriented to the sun and away from the sun appear brighter and darker, respectively, compared to a flat surface. These effects can clearly be observed if surface slopes exceed a certain threshold, e.g. 7◦. An accurate digital elevation model (DEM) of about the same spatial resolution as the pixel size of the instrument and a very accurate ortho-rectification are required to achieve a satisfactory topographic correction [32]. Otherwise DEM artefacts will appear in the product after topographic / atmospheric correction.

Sen2Cor does not perform a topographic correction in quasi-flat areas to avoid artefacts in the corrected scene. Terrain correction is only performed if the elevation difference in the granule is > 50 m or if at least 1% of the scene pixels have slope values > 6 degrees. All three thresholds are configurable by advanced users. If these threshold are violated, then Sen2Cor switches automatically to flat terrain processing despite a DEM was specified. In that case Sen2Cor writes a message about quasi-flat terrain processing into the processing report file.

While the ortho-rectification needs only the terrain elevation data, the atmospheric / topographic correction requires the following additional products derived from the DEM:

- map of DEM slope (unit degree) (mandatory),
- map of DEM aspect (unit degree) (mandatory),
- map of DEM topographically cast shadow (optional)
  recommended for steep terrain and/or low solar elevation
  (binary map: 1=no shadow pixel, 0=shadow pixel)
- map of sky view factor (optional).

The sky view factor is the fraction of the visible hemisphere, i.e. for a flat terrain the sky view factor is 1, and if 50% of the hemisphere is not visible then the sky view factor is 0.5. If the sky view factor map is not specified, it will be calculated within the topographic module using an approximation with the local slope angle θ_n of a pixel at position (x,y) [33].

$$V_{sky}(x,y) = cos^2(\theta_n(x,y)/2) = \frac{1\ +\ cos(\theta_n(x,y))}{2} \tag{0.25}$$

A more accurate method employs a ray tracing algorithm to calculate the sky view factor, e.g., [34, 35]. However, the accurate algorithm is only needed in case of terrain with steep slopes. The terrain view factor

$$V_t(x,y) = 1\ -\ V_{sky}(x,y) \tag{0.26}$$

follows from the sky view factor.

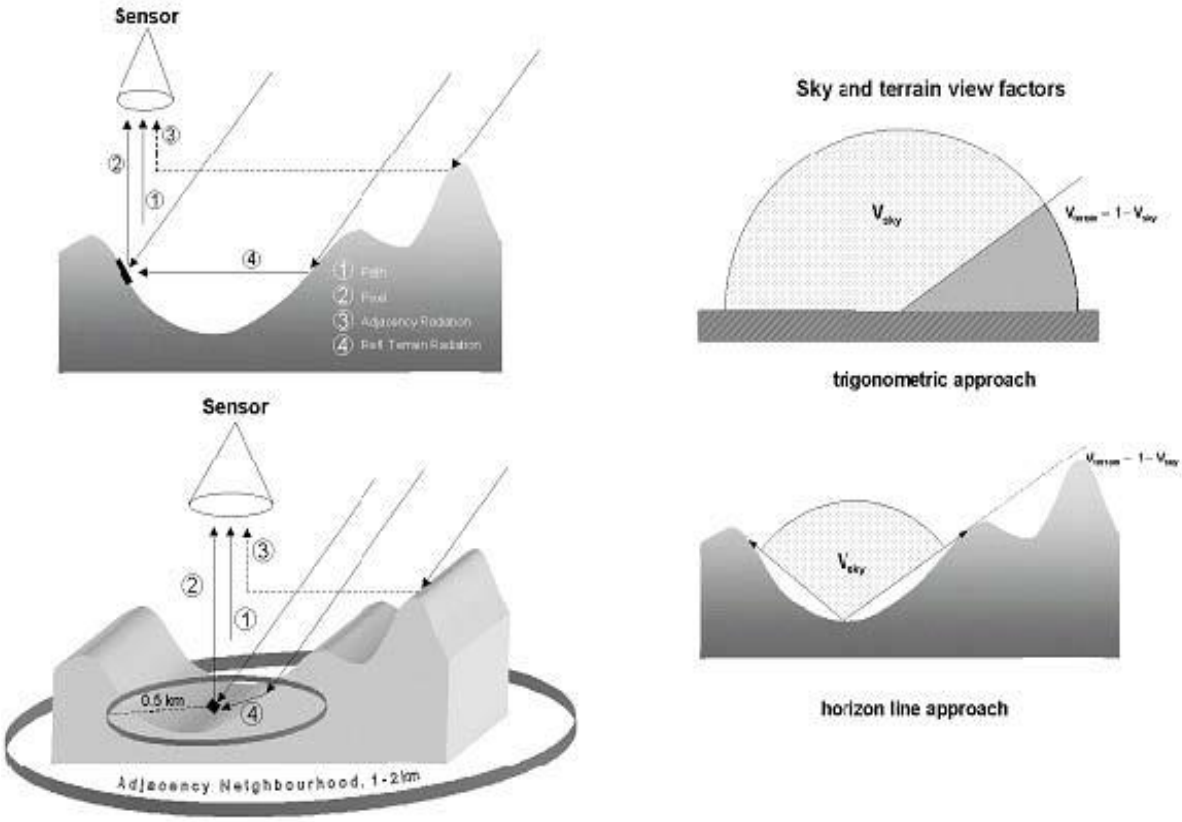

Figure 4-10 – Left: Radiation components in rugged terrain 1: path radiance; 2: pixel reflected radiance; 3: adjacency radiance; 4: reflected terrain radiance. Right: sky and terrain view factor

10 shows a sketch of the radiation components in a rugged terrain [32]. Compared to the flat terrain where the TOA radiance consists of three radiation components (path radiance, pixel reflected and adjacency radiation) one additional radiation component is needed in a rugged terrain, the terrain reflected radiation. The terrain reflected radiation is obtained from the average reflectance in a certain neighbourhood (radius 0.5 km) weighted with the terrain view factor and multiplied with the global solar flux.

Similar to the flat terrain case, the reflectance is calculated iteratively for each pixel of the image and for each band. The super-script index (i) denotes the iteration step:

$$\rho^{(i)}(x,y) = \frac{\pi \cdot \left(L(x,y) - L_p(z)\right)}{\tau_V(z) \cdot \left[E_{dir}(x,y,z) \ + E^*_{dif}(x,y,z) \ + E_t^{(i-1)}(z) \cdot \bar{\rho}^{(i-1)}_{terrain} \cdot V_t(x,y)\right]}$$

(0.27)

The terms are defined as:

$L(x,y)$	Measured radiance of georeferenced pixel;
$L_p(z)$	path radiance, dependent on elevation z and viewing geometry (θ_v, φ);
x, y	horizontal coordinates, corresponding to the georeferenced pixel positions;
z	vertical coordinate, containing the elevation information from the DEM;
θ_v	sensor view angle;
$\tau_V(z)$	total ground-to-sensor transmittance, dependent on sensor view angle θ_v, direct plus diffuse components, i.e., $\tau = \tau_{dir} + \tau_{dif}$;
$\tau_s^{dir}(z)$	sun-to-ground beam (direct) transmittance;
$E_{dir}(x,y,z)$	direct component of global solar flux on the ground (see equation (0.29));
$E^*_{dif}(x,y,z)$	diffuse hemispherical component of global solar flux on inclined plane (see equation (0.30));
$E_t(z)$	Radiation incident upon adjacent slopes;
E_s	extraterrestrial solar irradiance (earth-sun distance for d=1 astronomical unit);
$E_g(z)$	global flux (direct plus diffuse solar flux on a horizontal surf. at elevation z);
b(x,y)	binary cast shadow factor: b=1 if pixel receives direct solar beam, otherwise b=0;
$\beta(x, y)$	angle between the solar ray and the surface normal (illumination angle);
$\bar{\rho}^{(i)}_{terrain}(x,y)$	locally varying average terrain reflectance, calculated iteratively (i=1,2,3), initial value $\bar{\rho}^{(0)}_{terrain}$= 0.1;
$V_t(x, y)$	terrain view factor (range 0-1).

The solar and DEM geometry is shown in Figure 4-11 . If θ_s, θ_n, φ_s ,φ_n denote solar zenith angle, terrain slope angle, solar azimuth angle and topographic azimuth angle, respectively, the illumination angle β can be obtained from the DEM slope and aspect angles and the solar geometry:

$$\cos\beta(x,y) = \cos\theta_S \cdot \cos\theta_n(x,y) \ + \sin\theta_S \cdot \sin\theta_n(x,y) \cdot \cos\{\phi_S - \phi_n(x,y)\}$$

(0.28)

The direct component of global solar flux on the ground results from

$$E_{dir}(x,y,z) = b(x,y) \cdot E_S \cdot \tau_S(z) \cdot \cos\beta(x,y) \qquad (0.29)$$

and the diffuse solar flux on an inclined plane is calculated with Hay's model [36] taking also into account the binary topographic cast shadow factor b:

$$E^{*}_{dif}(x,y,z) = E_{dif}(z) \cdot \left[b(x,y) \cdot \tau_S^{dir}(z) \cdot \frac{\cos\beta(x,y)}{\cos\theta_S} + \left\{1 - b(x,y) \cdot \tau_S^{dir}(z)\right\} \cdot V_{sky}(x,y) \right] \tag{0.30}$$

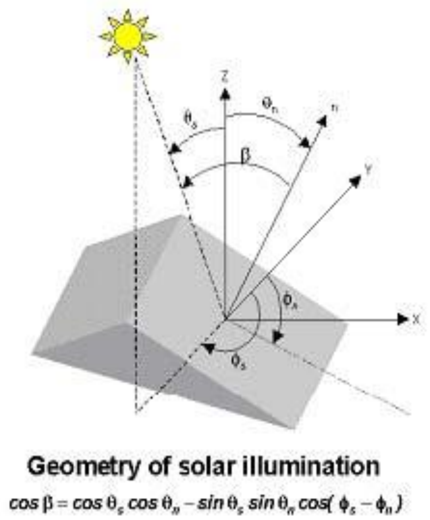

Figure 4-11 – Solar illumination geometry

First again the adjacency effect is neglected and surface reflection computation starts with a fixed terrain reflectance of $\bar{\rho}^{(0)}_{terrain} = 0.1$ [32]. The next step iterates equation (0.27) averaging the reflected terrain radiation over a square box of 0.5 × 0.5 km. If equation (0.27) is used with $E_t = E_g$ then three iterations are usually sufficient to be independent of the start value of the terrain reflectance [32]. However, for highly reflective surfaces, e.g. snow, and high terrain view factors, more than three iterations are necessary, and a faster convergence of $\bar{\rho}^{(i)}_{terrain}$ can be achieved with a geometric series for the terrain reflected radiation E_t as proposed in [37]:

$$E_t^{(i)} = E_g \, \frac{\bar{\rho}^{(i-1)}_{terrain} V_t}{1 \; - \; \bar{\rho}^{(i-1)}_{terrain} \; \bar{V}_t} \tag{0.31}$$

If these iterations are finished the last processing step accounts for the adjacency effect as in the case of flat terrain processing following equation (0.23).

4.8 Empirical BRDF correction

For many surface covers the reflectance increases with increasing solar zenith and / or viewing angle [38]. Scenes in mountainous regions often exhibit a large variation of terrain slopes, and thus bidirectional brightness variations for a certain surface cover, e.g. meadow or forest. This behaviour cannot be adequately eliminated with the Lambertian assumption. It leads to overcorrected reflectance values in faintly illuminated areas (having small values of *cosβ*), see Figure 4-12 (left). The central part of this Figure shows the result of an empirical correction with a simple geometric function depending on the local solar zenith angle β as explained below. Obviously, some correction is needed to avoid a misclassification of these bright overcorrected areas. Several approaches have been pursuit to solve this problem:

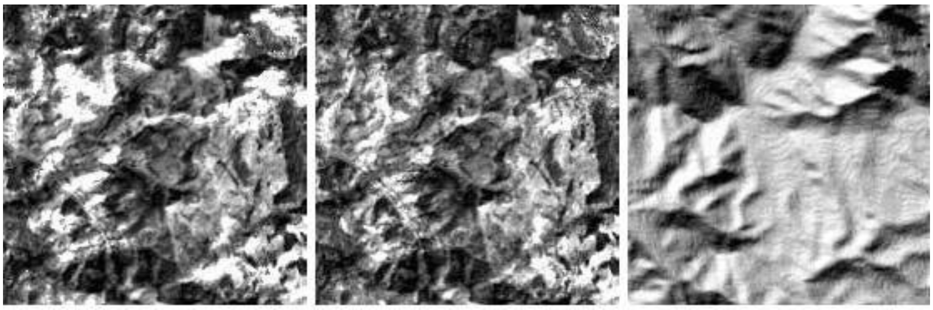

Figure 4-12 – BRDF correction in rugged terrain imagery
Left: image without BRDF correction.
Centre: after BRDF correction with threshold angle $\beta_T = 65°$.
Right: illumination map = cos β

- an empirical coefficient C is calculated based on a regression of brightness values and the local illumination angle derived from the DEM. The coefficient depends on scene content and wavelength [39, 40].
- the sun-canopy-sensor (SCS) geometry is employed in forested terrain instead of the solely terrain-based geometry [41].
- the SCS method is coupled with the C-correction [42].
- a simplified empirical approach accounting for the direct and diffuse illumination and incidence and exitance angles applied to vegetation canopies [43].

These approaches produced good results on sample scenes with uniform cover types presented in the above papers. When applying the methods to a wider range of areas, some of the practical problems are:

- mountainous scenes often contain a number of different covers, e.g., deciduous forest, coniferous forest, mixed forest, shrubs, meadow, rocks, etc.
- the computation of the C coefficients for different surface covers would require a pre -classification.
- the correlation obtained for the C coefficients is often less than 0.7, yielding unreliable results with this method.

These remarks are supported by reference [40]. These authors applied different correction approaches to a TM scene containing different cover types and noted that there is no optimum method for all cover types. A drawback of the Minnaert and empirical C-methods is that they do not distinguish between the direct and diffuse solar illumination as opposed to the physically based approach of SEN2COR. Nevertheless, the latter approach also cannot avoid problems in faintly illuminated areas. Therefore, it is supplemented by an empirical method with three adjustable parameters (β_T, *b*, and *g*) as explained below. This approach was tested on different rugged terrain scenes with vegetated and arid landscapes and usually yields satisfactory results. It reduces overcorrected reflectance values starting at a threshold local solar zenith angle β_T which is greater than the scene's solar zenith angle θ_s.

Equation (0.32) defines the implemented basic geometric correction function which depends on the local solar incidence angle (solar illumination β_i) and the adjustable threshold angle β_T. The exponent b (= 1/3, 1/2, 3/4, or 1) is the second parameter which can be selected by the user. Some guidelines on the choice of b are discussed below. The third adjustable parameter is the lower bound g of the correction function, see Figure 4-13.

$$G = \left\{\frac{\cos\beta_i}{\cos\beta_T}\right\}^b \geq g \tag{0.32}$$

The threshold illumination angle β_T should have some margin to the solar zenith angle to retain the original natural variation of pixels with illumination angles close to the solar zenith angle. The threshold angle can be specified by the user and the following empirical rules are recommended:

- *if $\theta_s < 45^\circ$:* $\beta_T = \theta_s + 20^\circ$
- if $45 \leq \theta_s \leq 20^\circ$: $\beta_T = \theta_s + 15^\circ$
- if $\theta_s > 55^\circ$: $\beta_T = \theta_s + 10^\circ$

These rules are automatically applied by Sen2Cor.

The geometric function G needs a lower bound g to prevent a too strong reduction of reflectance values. Values of G greater than 1 are set to 1, and values less than the boundary g are reset to g. This means the processing works in the geometric regime from β_T to 90° and the updated reflectance is

$$\rho_g = \rho_L \cdot G \tag{0.33}$$

where ρ_L is the isotropic (Lambert) value.

Figure 4-13 shows a graphical presentation of equation (0.32). The left part displays the function G for different values of the exponent b. For b=1 the decrease with β_i is strong with a constant gradient. For smaller values of b the decrease with β_i is moderate initially, but the gradient increases with larger β_i. Currently, different functions G for soil/sand and vegetation can be selected in SEN2COR [S2-L2A-IODD]. The function G for soil/sand is applied with a wavelength-independent exponent b. After testing a large number of vegetated mountainous scenes two vegetation modes were finally selected because of their good performance:

1. b=0.75 for bands with λ< 720 nm and b=0.33 for λ> 720 nm ("weak" correction),

2. b=0.75 (λ< 720 nm) and b=1 (λ> 720 nm), ("strong" correction).

In most of the tested cases, the first vegetation mode ("weak" correction) was appropriate. A simple criterion (vegetation index $\rho_{850nm}/\rho_{660nm}$ > 3) is used to distinguish soil/sand and vegetation. The right part of Figure 4-13 shows the effect of shifting the threshold illumination angle β_T . For larger values of β_T the decline of function G starts later with a larger gradient, and the lower bound g is met at slightly higher values of β_i. In most cases, g=0.2 to 0.25 is adequate, in extreme cases of overcorrection g=0.1 should be applied.

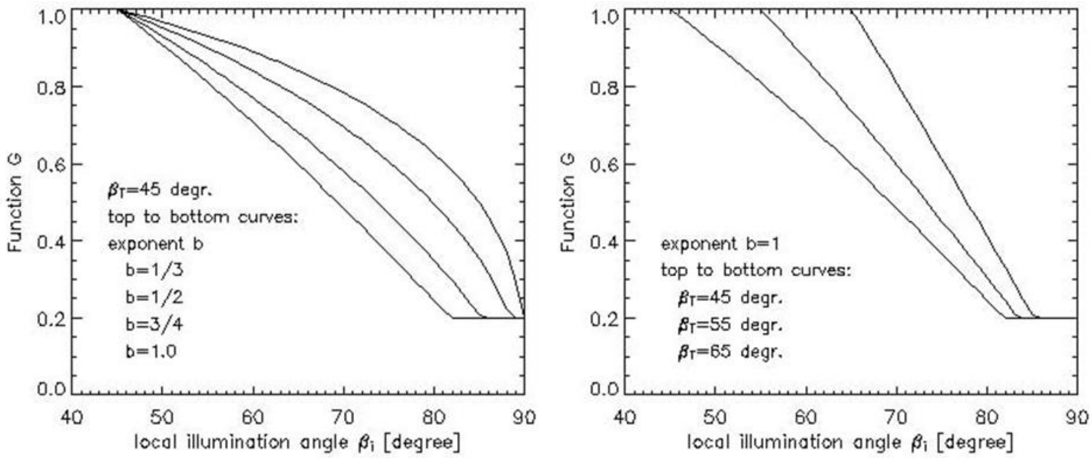

Figure 4-13 – Geometric functions for empirical BRDF correction

Left: Functions G of equation (0.32) for different values of the exponent b.
Right: Functions G of equation (0.32) for b=1 and different start values of β_T.
The lower cut-off value is g=0.2.

Reference [44] contains a comparison of different topographic correction methods for several Landsat-TM, ETM+, and SPOT-5 scenes from different areas. The proposed empirical Sen2Cor approach performed best in most of these cases, but no method ranked first in all cases.

There are two configuration options in the configuration file L2A_GIPP.xml with respect to BRDF correction. BRDF correction is switched off by default (value 0). The user may switch on BRDF correction selecting a correction model (values 1,2, 11,12, 21,22). Correction models 1 and 2 refer to using the simple correction function (0.34) with b=1 resp. b=0.5. Correction models 11 and 12 are equal to correction model 1 with b=1 for soil/sand and perform a 'week' resp. a 'strong' correction for vegetation. Correction models 21 and 22 are equal to correction model 2 with b=0.5 for soil/sand and perform a 'week' resp. a 'strong' correction for vegetation. Correction model 21 is the recommended one if switching on BRDF correction yielding good results in most cases. The second parameter for user configuration is the lower boundary of BRDF correction factor g (Default g=0.22).

4.9 Algorithm validation

The AC algorithms proposed in this document derive from ATCOR [45] and were continually validated over a time period of more than 10 years. Comparisons were conducted with in-situ reflectance measurements, mainly during EU and ESA campaigns [46-48]. The validations comprised a large range of surface covers, atmospheric conditions, and solar geometries. Sen2Cor also participated in Atmospheric Correction Intercomparison eXercise ACIX-1 [49] and ACIX-2/CMIX [50]. Recent results of performance assessment of Sen2Cor are published monthly in the L2A-Quality reports, accessible at:

https://sentinels.copernicus.eu/documents/247904/685211/Sentinel-2-L2A-Data-Quality-Report [51].

APPENDIX A Bibliography

1. Mayer, B. and A. Kylling, *The libRadtran software package for radiative transfer calculations*. 2016.
2. Mayer, B., et al., *libRadtran user's guide*. 2019.
3. Sentinel-2 MPC Team. *Sentinel-2 L1C Data Quality Report (S2-PDGS-MPC-L1CDQR)*. 11 June 2020]; Available from: https://earth.esa.int/web/sentinel/user-guides/sentinel-2-msi/document-library/.
4. European Space Agency. *Sentinel-2 Spectral Response Functions (S2-SRF)*. 2017, COPE-GSEG-EOPG-TN-15-0007; Version 3.0, Available from: https://sentinels.copernicus.eu/web/sentinel/user-guides/sentinel-2-msi/document-library/-/asset_publisher/Wk0TKajiISaR/content/sentinel-2a-spectral-responses. Accesed: 11.06.2020.
5. Berk, A., et al., *MODTRAN4 USER'S MANUAL*. 1999, Air Force Research Laboratory, Space Vehicles Directorate, Air Force Materiel Command: Hanscom AFB, MA 01731-3010.
6. Schlapfer, D., et al., *Atmospheric precorrected differential absorption technique to retrieve columnar water vapor.* Remote Sensing of Environment, 1998. **65**(3): p. 353-366.
7. Irish, R.R., *Landsat 7 automatic cloud cover assessment.* Algorithms for Multispectral, Hyperspectral, and Ultraspectral Imagery Vi, 2000. **4049**: p. 348-355.
8. Irish, R.R., et al., *Characterization of the Landsat-7 ETM+ automated cloud-cover assessment (ACCA) algorithm.* Photogrammetric Engineering and Remote Sensing, 2006. **72**(10): p. 1179-1188.
9. Hall, D.K. and G.A. Riggs. *Normalized-Difference Snow Index (NDSI)*. 2010, Available from: https://ntrs.nasa.gov/citations/20100031195.pdf. Accesed: 2.10.2020.
10. U.S. Geological Survey. *L7 Irish Cloud Validation Masks*. 2016, doi: 10.5066/F7XD0ZWC, Available from: https://landsat.usgs.gov/landsat-7-cloud-cover-assessment-validation-data. Accesed: 2.10.2020.
11. Emde, C., et al., *The libRadtran software package for radiative transfer calculations (version 2.0.1).* Geoscientific Model Development, 2016. **9**(5): p. 1647-1672.
12. Stamnes, K., et al., *Numerically Stable Algorithm for Discrete-Ordinate-Method Radiative-Transfer in Multiple-Scattering and Emitting Layered Media.* Applied Optics, 1988. **27**(12): p. 2502-2509.
13. Nicodemus, F.E., *REFLECTANCE NOMENCLATURE AND DIRECTIONAL REFLECTANCE AND EMISSIVITY.* Applied Optics, 1970. **9**(6): p. 1474-+.
14. Slater, P.N., *RADIOMETRIC CONSIDERATIONS IN REMOTE-SENSING.* Proceedings of the Ieee, 1985. **73**(6): p. 997-1011.
15. Schaepman-Strub, G., et al., *Reflectance quantities in optical remote sensing-definitions and case studies.* Remote Sensing of Environment, 2006. **103**(1): p. 27-42.
16. Tanre, D., M. Herman, and P.Y. Deschamps, *Influence of the Background Contribution Upon Space Measurements of Ground Reflectance.* Applied Optics, 1981. **20**(20): p. 3676-3684.

17. Kaufman, Y.J., *The Atmospheric Effect on the Separability of Field Classes Measured from Satellites.* Remote Sensing of Environment, 1985. **18**(1): p. 21-34.
18. Gao, B.C., et al., *Correction of thin cirrus path radiances in the 0.4-1.0 mu m spectral region using the sensitive 1.375 mu m cirrus detecting channel.* Journal of Geophysical Research-Atmospheres, 1998. **103**(D24): p. 32169-32176.
19. Gao, B.C., et al., *An algorithm using visible and 1.38-mu m channels to retrieve cirrus cloud reflectances from aircraft and satellite data.* Ieee Transactions on Geoscience and Remote Sensing, 2002. **40**(8): p. 1659-1668.
20. Gao, B.C., K. Meyer, and P. Yang, *A new concept on remote sensing of cirrus optical depth and effective ice particle size using strong water vapor absorption channels near 1.38 and 1.88 mu m.* Ieee Transactions on Geoscience and Remote Sensing, 2004. **42**(9): p. 1891-1899.
21. Richter, R., et al., *Correction of cirrus effects in Sentinel-2 type of imagery.* International Journal of Remote Sensing, 2011. **32**(10): p. 2931-2941.
22. Kaufman, Y.J., et al., *The MODIS 2.1-mu m channel - Correlation with visible reflectance for use in remote sensing of aerosol.* Ieee Transactions on Geoscience and Remote Sensing, 1997. **35**(5): p. 1286-1298.
23. Kaufman, Y.J. and C. Sendra, *Algorithm for Automatic Atmospheric Corrections to Visible and near-Ir Satellite Imagery.* International Journal of Remote Sensing, 1988. **9**(8): p. 1357-1381.
24. Liang, S.L., et al., *An operational atmospheric correction algorithm for Landsat Thematic Mapper imagery over the land.* Journal of Geophysical Research-Atmospheres, 1997. **102**(D14): p. 17173-17186.
25. Louis, J., et al., *Integration and Assimilation of Meteorological (Ecmwf) Aerosol Estimates into Sen2cor Atmospheric Correction.* Igarss 2018 - 2018 Ieee International Geoscience and Remote Sensing Symposium, 2018: p. 1894-1897.
26. Levy, R.C., et al., *Algorithm for remote sensing of tropospheric aerosol over dark targets from MODIS: Collections 005 and 051, Revision 2*. 2009.
27. Santer, R., et al., *A surface reflectance model for aerosol remote sensing over land.* International Journal of Remote Sensing, 2007. **28**(3-4): p. 737-760.
28. Kaufman, Y.J., et al., *Operational remote sensing of tropospheric aerosol over land from EOS moderate resolution imaging spectroradiometer.* Journal of Geophysical Research-Atmospheres, 1997. **102**(D14): p. 17051-17067.
29. ECMWF. *Copernicus Atmosphere Monitoring Service*. Available from: http://atmosphere.copernicus.eu/. Accesed: 9. February 2018.
30. Richter, R. and D. Schlapfer, *Considerations on water vapor and surface reflectance retrievals for a spaceborne imaging spectrometer.* Ieee Transactions on Geoscience and Remote Sensing, 2008. **46**(7): p. 1958-1966.
31. Thuillier, G., et al., *The solar spectral irradiance from 200 to 2400 nm as measured by the SOLSPEC spectrometer from the ATLAS and EURECA missions.* Solar Physics, 2003. **214**(1): p. 1-22.

32. Richter, R., *Correction of satellite imagery over mountainous terrain.* Applied Optics, 1998. **37**(18): p. 4004-4015.
33. Kondratyev, K.Y., *Radiation in the Atmosphere*. International Geophysics. Vol. 12. 1969, London: Academic Press.
34. Dozier, J., J. Bruno, and P. Downey, *A Faster Solution to the Horizon Problem.* Computers & Geosciences, 1981. **7**(2): p. 145-151.
35. Corripio, J.G., *Vectorial algebra algorithms for calculating terrain parameters from DEMs and solar radiation modelling in mountainous terrain.* International Journal of Geographical Information Science, 2003. **17**(1): p. 1-23.
36. Hay, J.E. and D.C. McKay, *Estimating Solar Irradiance on Inclined Surfaces: A Review and Assessment of Methodologies.* International Journal of Solar Energy, 1985. **3**(4-5): p. 203-240.
37. Sirguey, P., *Simple correction of multiple reflection effects in rugged terrain.* International Journal of Remote Sensing, 2009. **30**(4): p. 1075-1081.
38. Kriebel, K.T., *Measured Spectral Bidirectional Reflection Properties of 4 Vegetated Surfaces.* Applied Optics, 1978. **17**(2): p. 253-259.
39. Teillet, P.M., B. Guindon, and D.G. Goodenough, *On the Slope-Aspect Correction of Multispectral Scanner Data.* Canadian Journal of Remote Sensing, 1982. **8**(2): p. 84-106.
40. Riano, D., et al., *Assessment of different topographic corrections in Landsat-TM data for mapping vegetation types (2003).* Ieee Transactions on Geoscience and Remote Sensing, 2003. **41**(5): p. 1056-1061.
41. Gu, D. and A. Gillespie, *Topographic normalization of landsat TM images of forest based on subpixel Sun-canopy-sensor geometry.* Remote Sensing of Environment, 1998. **64**(2): p. 166-175.
42. Soenen, S.A., D.R. Peddle, and C.A. Coburn, *SCS+C: A modified sun-canopy-sensor topographic correction in forested terrain.* Ieee Transactions on Geoscience and Remote Sensing, 2005. **43**(9): p. 2148-2159.
43. Shepherd, J.D. and J.R. Dymond, *Correcting satellite imagery for the variance of reflectance and illumination with topography.* International Journal of Remote Sensing, 2003. **24**(17): p. 3503-3514.
44. Richter, R., T. Kellenberger, and H. Kaufmann, *Comparison of Topographic Correction Methods.* Remote Sensing, 2009. **1**(3): p. 184-196.
45. Richter, R., D. Schlapfer, and A. Muller, *An automatic atmospheric correction algorithm for visible/NIR imagery.* International Journal of Remote Sensing, 2006. **27**(9-10): p. 2077-2085.
46. European Space Agency, *ESA DAISEX (digital Airborne Spectrometer Experiment) Final Results Workshop: Proceedings*. 2001: ESA.
47. Richter, R., A. Muller, and U. Heiden, *Aspects of operational atmospheric correction of hyperspectral imagery.* International Journal of Remote Sensing, 2002. **23**(1): p. 145-157.
48. Richter, R. and D. Schlapfer, *Geo-atmospheric processing of airborne imaging spectrometry data. Part 2: atmospheric/topographic correction.* International Journal of Remote Sensing, 2002. **23**(13): p. 2631-2649.
49. Doxani, G., et al., *Atmospheric Correction Inter-Comparison Exercise.* Remote Sensing, 2018. **10**(2).

50. Vermote, E., et al., *ACIX – Atmospheric Atmospheric Correction Inter-comparison eXercise*, in *IGARSS 2019 - 2019 IEEE International Geoscience and Remote Sensing Symposium*. 2019. p. 8493-8496 %@ 2153-6996.

51. Sentinel-2 MPC Team. *Sentinel-2 L2A Data Quality Report (S2-PDGS-MPC-L2ADQR)*. 18 August 2020]; Available from: https://earth.esa.int/web/sentinel/user-guides/sentinel-2-msi/document-library/.